Chapter 4
High Temperature Cuprate Superconductors and Later Discoveries

Abstract The discovery of superconductivity at 30 K in an oxygen deficient $La_4Ba_1Cu_5O_{5(3-y)}$ compound by Bednorz and Muller in 1986 lifted the despondency under which the superconductivity community was reeling since 1973 when highest $T_c = 23$ K was recorded in sputtered Nb_3Ge films and T_c went no further. Chu raised T_c of this compound to 40 K by applying pressure and Cava to 36 K after substituting Sr at the La-site. A breakthrough came in early 1987 when Wu and Chu announced a record $T_c = 93$ K in $Y_1Ba_2\ Cu_3\ O_7$. T_c thus crossed the 77 K mark first time. Soon Maeda discovered superconductivity at 110 K in another cuprate of the type $Bi_2Sr_2Ca_2Cu_3O_{10}$ (Bi-2223 with 3 CuO_2 layers). T_c thus increases with the number of CuO_2 layers but not beyond three layers. These layered curates have large anisotropy. The superconductivity is strong in the *a-b* planes (CuO_2 layers) and weak along the *c*-axis. Critical parameters B_{c2} and J_c too are high in the *a-b* plane and low along *c*-direction. Both the materials, Bi-2223 and YBCO are produced commercially and used for selected applications. The new improved 2G-YBCO wires are coated multilayered thin film conductors produced by employing sophisticated techniques and getting popularity among the community. Two more cuprates with still higher T_c and analogous to Bi-system were discovered. A $T_c = 125$ in $Tl_2Ca_2Ba_2Cu_3O_x$ (Ti-2223) and 135 K in $Hg_1Ba_2Ca_2Cu_3O_{6+\delta}$ (Hg-1223) were reported. These materials were, however, not pursued for commercial production because of the toxicity involved. Superconductivity was also found in 2001 in MgB_2 at 39 K, easily attainable with the use of a cryo-cooler. Besides, the material is quite cheap. MgB_2 has two energy gaps and appears to be a BCS superconductor. It is being produced commercially now. The chapter also reviews all the discoveries that took place in 2008 onwards. Hosano reported superconductivity in iron based oxy-pnictides of the type LaFeAsO(1111) around 25 K. T_c in excess of 50 K were reported in Sm and Nd based pnictides. The strategy adopted to enhance T_c has been to dope the insulating La_2O_2 layer suitably whereby a charge, electron/hole is transferred to the Fe_2As_2 conduction layer. Thus a $T_c = 38$ K was reported in a K-doped $(Ba_{0.6}K_{0.4})\ Fe_2As_2$ compound. Very strange behavior of the appearance, disappearance and re-appearance of superconductivity with increasing pressure was announced in an

© Springer International Publishing Switzerland 2015

R.G. Sharma, *Superconductivity*, Springer Series in Materials Science 214,
DOI 10.1007/978-3-319-13713-1_4

iron-chalcogenide, $Tl_{0.6}Rb_{0.4}Fe_{1.67}Se_2$ hinting at the possibility of two different types of superconducting phases appearing at different pressures. A maximum T_c = 48 K was obtained in this material at a pressure of 12.4 GPa.

4.1 Discoveries of High T_c Cuprate Superconductors: Discovery of Superconductivity in La–Ba–Cu–O System (T_c = 35 K)

The search for superconductivity among the elements in the periodical table, in alloys and compounds continued unabated after the discovery of this fascinating phenomenon. Superconductivity was indeed discovered in a variety of families (listed in Table 4.1) but the T_c still remained confined to low value, necessitating the use of liquid helium for operation. The highest T_c was obtained in 1973–1974 in thin films of Nb_3Ge by Gavaler [1] and Tastardi et al. [2] by optimizing the deposition parameters. There was a lull for next 12 years until in 1986 all of a sudden, something very unusual happened. Two research scientists at IBM, Zűrich, namely, Bednorz and Muller discovered [3] superconductivity at 30 K in an oxide compound of the type $La_{5-x}Ba_xCu_5O_{5(3-y)}$. The compound was prepared by co-precipitation of the nitrates of La, Ba and Cu taken in appropriate ratios. This was followed by the solid state reaction at 900 °C in a reduced atmosphere. Samples were finally prepared in the form of pellets sintered at 900 °C. The resistivity behaviour of these samples is shown in Fig. 4.1. Clearly, the resistivity drops with the fall of temperature nearly linearly, then rises logarithmically and then drops sharply by three orders of magnitude. The onset transition temperature is 30 K. Three phases were detected in the material. (i) a cubic phase dependent upon Ba composition, (ii) a superconducting phase $La_{1.8}Ba_{0.2}$ CuO_4 and a third (iii) Perovskite layered phase of the type K_2NiF_4 with a = 3.79 Å and c = 13.2 Å. The resistivity was found to be changing with measuring sample current indicating that the superconductivity is granular in nature. The material turns out to be an O^{2-} deficient phase with mixed valence Cu constituents, namely Jahn-Teller ions Cu^{2+} and non Jahn-Teller ions Cu^{3+} resulting in a large λ (the electron-phonon coupling parameter) and large metallic conductivity. The ideal perovskite La_2CuO_4 structure shown in Fig. 4.2 is orthorhombic at room temperature and becomes tetragonal at 500 K. Pure La_2CuO_4 is insulating and antiferromagnetic with a Neel temperature of 290 K. Ba and Sr substitute at La sites and the compound $La_{2-x}M_xCuO_4$ shows a T_c of 35 K at M = 0.15 and 0.2 for Ba and Sr respectively. The doped material has a tetragonal structure at room temperature and turns orthorhombic at 180 K. It was not the first time that superconductivity was observed in oxides. As early as 1973, Johnston et al. [4] reported superconductivity in a Li–Ti–O system with a T_c = 13.7 K. The X-ray analysis showed the presence of three crystallographic phases. One phase with a spinel structure had the highest T_c with a comparatively

Table 4.1 Different families of superconductors with corresponding T_c values (most values from [8], with permission from R.P. Aloysius)

Sr no.	Type of superconductor	Example	Max. T_c (K)
1	Pure elements	Nb	9.2
2	Transition metal alloys	MoRe	12
3	Carbides	NbC	11
4	Nitrides	NbN	15
5	Amorphous superconductors	VGa	8.4
6	Nitrocarbides	$NbN_{0.7}C_{0.3}$	18
7	Laves phase (C-15 structure)	$CeRu_2$	6.1
8	Cheveral phase	$PbMo_6S_8$	12–14
9	A-15 (β-Tungsten)	Nb_3Sn–Nb_3Ge	18–23
10	Organic superconductors	$(TMTSF)_2PF_6$	1 (at 12 kbar)
11	Intercalated superconductors	$TaS_2(C_5H_5N)_{1/2}$	3.5
12	Heavy fermionic superconductors	UPt_3–$CeCoIn_5$	0.48–2.3
13	Magnetic superconductors	$ErRh_4B_4$	8.6
14	Semi-metal superconductors	La_3Se_4	10
15	First oxide superconductors	$BiPb_{1-x}Bi_xO_3$	13 (x = 0.25)
16	K-doped Ba–Bi oxide, supercond.	$(Ba_{0.6}K_{0.4})BiO_3$	31.5
17	Boro-carbides	YNi_2B_2C	15
18	Rare earth cuperates	$YBa_2Cu_3O_{7-\delta}$	92
19	Lanthenate (discovery of high T_c superconductor)	$La_{5-x}Ba_xCu_5O_{5(3-y)}$	35
20	Bismuth oxide superconductors (Bi-2223)	$Bi_{1.7}Pb_{0.4}Sr_{1.8}Ca_2Cu_{3.5}O_y$	110
21	Mercury oxide superconductors (Hg-1223)	$HgBa_2Ca_2Cu_3O_{8+\delta}$	155 (15 GPa)
22	Thallium oxide superconductors (Tl-2223)	$Tl_2Ca_2Ba_2Cu_3O_x$	125
23	Fullerides	Rb_2C_{60}	45
24	Magnesium diboride	MgB_2	39
25	Iron pnictides	$NdFeAsO_{0.82}F_{0.18}$	51
26	F-doped La–Fe–As compounds	$NdFeAsO_{0.82}F_{0.18}$	55 K
27	Iron chalcogenides	$Tl_{0.6}Rb_{0.4}Fe_{1.67}Se_2$	33

low carrier concentration of n = 2–4 × 10^{21}/cm^3. Soon after Sleight et al. [5] reported a T_c = 13 K in a mixed valence Ba $Pb_{1-x}Bi_xO_3$ system which also has a perovskite structure. Strong electron phonon coupling was believed to be responsible for superconductivity. Prior to the discovery by Bednorz and Muller, scientists had almost given-up hopes of achieving high T_c in superconductors under the belief of the theoretical predictions made around the time. On the basis of the BCS theory even with highest values of the electron density of state and the electron-phonon coupling parameter, the T_c would not go beyond 30 K. What happened after the publication of the celebrated paper by Bednorz and Muller was something

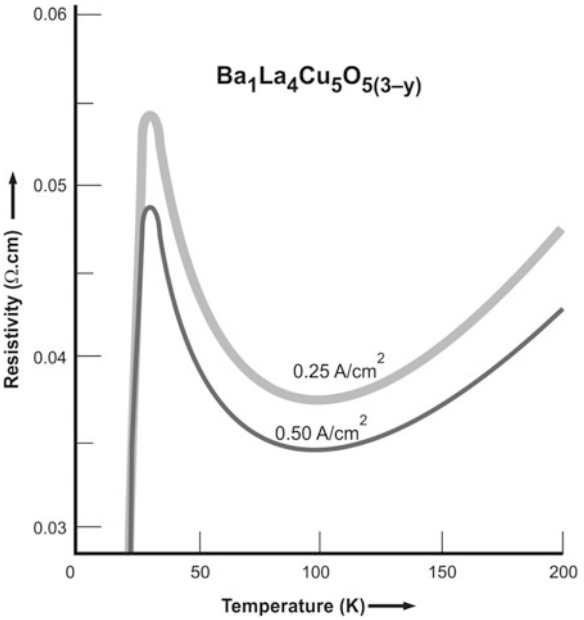

Fig. 4.1 Electrical resistivity plotted against temperature for the compound $Ba_1La_4Cu_5O_{5(3-y)}$. Superconducting transition occurs at $\sim$30 K and the resistivity shows variation with measuring current [3] (With kind permission of Springer Science+Business Media)

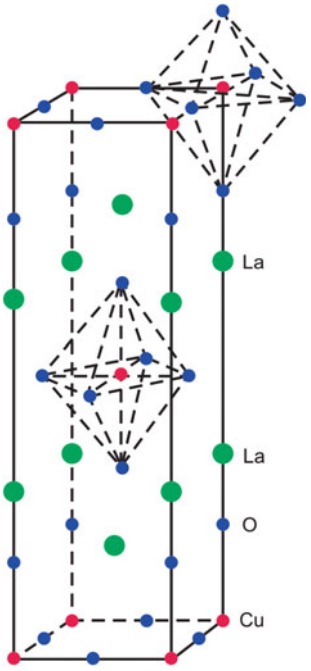

Fig. 4.2 The ideal La_2CuO_4 (K_2NiF_4) crystal structure. Superconductivity sets in with Ba/Sr substitution at the La site

unprecedented and quite unexpected. Superconductivity was reported in oxide systems one after another with higher and higher transition temperature, climbing well above the liquid nitrogen temperature (77 K). Within a couple of years T_c rose to as high as 150 K making the T_c/Year graph rising almost exponentially (Fig. 4.3).

Chu et al. [6] at the university of Houston raised the T_c of the compound $(La_{0.85}Ba_{0.15})_2CuO_{4-y}$ from 36 K at ambient pressure to 40 K after applying a pressure of 13 kbar. Cava et al. [7] on the other hand partially replaced La by Strontium (smaller ion) replicating chemical pressure. The compound studied had the chemical composition $La_{1.8}Sr_{0.2}CuO_4$. Undoped La_2CuO_4 structure is slightly orthorhombic distortion of K_2NiF_4, all the copper ions are in Cu^{2+} state and no superconductivity is observed down to 4.2 K. Substitution of La by Sr stabilizes tetragonal undistorted K_2NiF_4 and oxidizes some Cu to Cu^{3+} state resulting in a mixed valence compound. The compound had been annealed in air as well as in oxygen [7]. Sample annealed in air reveals the presence of a mixture of a metallic phase, a semiconducting phase and a superconducting phase. Oxygen anneal on the other hand leads to a metallic and a superconducting phase. Oxygen anneal also improves the onset T_c from 36.5 to 38.5 K. Thus Sr and oxygen both are important for the oxidizing condition. Oxygen pressure influences Cu^{3+}/Cu^{2+} valence ratio as well as charge compensation by O-vacancies.

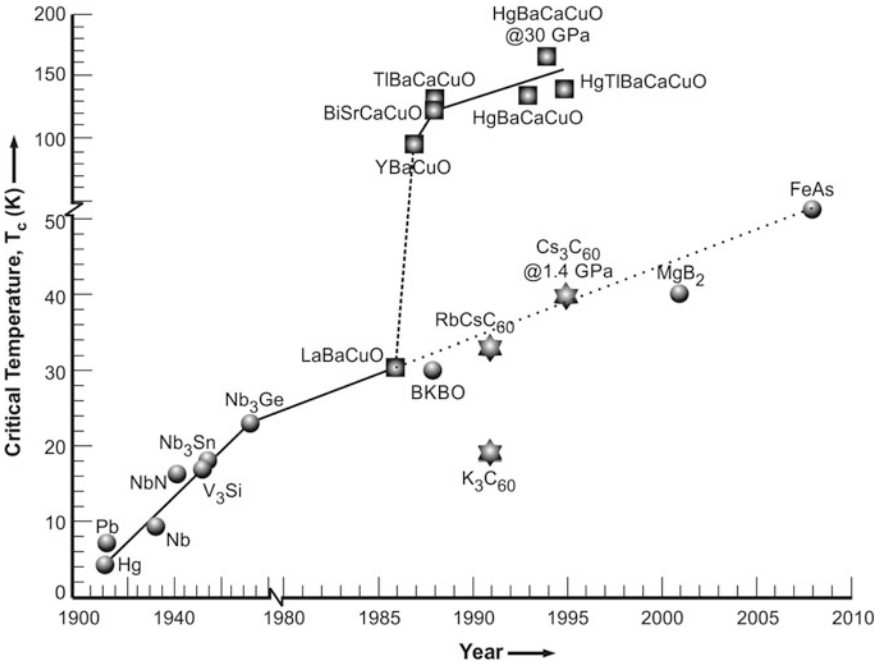

Fig. 4.3 Transition temperatures of important elements, alloys and compounds plotted against the year of their discovery. The *curve* rose sharply in 1986 when high T_c cuprates were discovered

The discovery of superconductivity by Bednorz and Műller in an oxide system opened the flood gate to the discovery of a larger family of oxide systems containing copper. Many superconductors containing Cu–O layers, now called cuprates with higher and higher T_c values rising far above the boiling temperature of nitrogen, 77 K were discovered. This evoked great excitement among the scientific community of all shades who hoped that an engineering revolution will soon take place where the conventional superconductors used in large scale applications will be replaced by these oxide superconductors. Although the hope of using these superconductors at 77 K for producing high magnetic fields is yet to be realized, yet selected cuprates have been produced commercially and are being increasingly used in a variety of power applications where high current densities in presence of high magnetic field are not required. They have nevertheless been found suitable for high field production, when operated below 65 K. A vast family of cuprate superconductors is tabulated along with their T_c values in Table 4.2.

Below we briefly discuss the discovery of important superconductors which surpassed the T_c of the previous superconductors.

4.2 The Y–Ba–Cu–O (YBCO) System—First Superconductor with T_c Above 77 K

A real breakthrough occurred in the history of superconductivity in March 1987 when Wu et al. [9] discovered superconductivity in a $Y_1Ba_2Cu_3O_{7-x}$ (or simply YBCO or also called just Y123) system at 93 K making it possible first time to cool down a superconductor below its T_c using liquid nitrogen instead of liquid helium. Figure 4.4 shows the resistivity—temperature plots at different magnetic field reported by Wu et al. [9]. The superconducting phase was identified to be $Y_1Ba_2Cu_3O_7$ which is an oxygen deficient triplet perovskite unit cell of the type ABO_3. The triplet cell would have been $(Y_1Ba_2)Cu_3O_9$ but the superconducting phase is oxygen deficient that is, $Y_1Ba_2Cu_3O_7$ and has a T_c = 93 K. $Y_1Ba_2Cu_3O_7$ has an orthorhombic distorted structure and is shown in Fig. 4.5. Clearly Cu ion has two distinct crystallographic and dissimilar sites Cu(1) and Cu(2). Cu(1) is surrounded by a squashed square planar O configuration in the *b*-*c* plane and linked to similar sites in a one dimension along the *b*-axis. Cu(2) site is 5 coordinated by a square pyramidal arrangement of O. The vertex of the pyramid is at O(4) site along the *c*-axis. The Y ion is at the centre of the two Cu–O sheets eight O-coordinated and Ba ten O-coordinated. We thus find that Cu–O network is important for cuprates. Cu(1)–O(1) chains are crucial to superconductivity in this material. Cu(2)–O(2)/O(3) do not seem to be so crucial for 90 K transition. Cu(1)–O(4) bond is much stronger than Cu(1)–O(1), bond lengths being 1.85 and 1.943 Å respectively. Oxygen vacancies occur in O(1) sites easily which

Table 4.2 A large variety of cuprate superconductors with their T_c values

Sr. no.	Compound	T_c (K)
1	$La_{1.85}(Ba/Sr)_{0.15}CuO_4$	35
2	$La_2CuO_{4+\delta}$	45
3	$La_{1.6}Sr_{0.4}CaCu_2O_{6+\delta}$	60
4	$Y_1Ba_2Cu_3O_7$	92
5	$Y_1Ba_2Cu_3O_8$	82
6	$TlBa_2Ca_{n-1}Cu_nO_{2n+3}$	120 (n = 3)
7	$TlBa_2Ca_{n-1}Cu_nO_{2n+4}$	127 (n = 3)
8	$Bi_2Sr_2Ca_{n-1}Cu_nO_{2n+4}$	110 (n = 3)
9	$HgBa_2Ca_{n-1}Cu_nO_{2n+2+\delta}$	134 (n = 3)
10	$CuBa_2Ca_{n-1}Cu_nO_7$	120
11	$Sr_2Ca_{n-1}Cu_nO_4$	90
12	$Pb_2Sr_2(Ca, Y, Nd)Cu_3O_8$	70
13	$Pb_2(Sr, La)_2Cu_2O_6$	32
14	$PbBaSrYCu_3O_8$	50
15	$(Pb, Cu)(Ba, Sr)_2(Y, Ca)Cu_2O_7$	53
16	$Pb_{0.5}Sr_{2.5}(Y, Ca)Cu_2O_7$	104
17	$(Pb, Cu)(Sr, La)_2CuO_5$	32
18	$(Nd, Ce)_2CuO_{4-\delta}$	24
19	$(Nd, Ce, Sr)CuO_{4-\delta}$	28
20	$(Pb, Cu, Eu, Ce)_2(Sr, Eu)_2Cu_2O_9$	25
21	$(EuCe)_2(Ba, Eu)_2Cu_3O_{10}$	43
22	$Bi_2Sr_2(Gd, Ce)_2Cu_2(CO_3)O_7$	34
23	$Tl_{0.5}Pb_{0.5}Sr_4Cu_2(CO_3)O_7$	70
24	$(BaSr)_2CuO_2(CO_3)$	40
25	$Sr_{4-x}Ba_xTlCu_2(CO_3)O_7$	62
26	$Tl_{0.5}Pb_{0.5}Sr_2Gd_{2-x}Ce_xCu_2O_{9-\delta}$	45
27	$NbSr_2(Gd, Ce)_2Cu_2O_y$	27
28	$Bi_2Sr_{6-x}Cu_3O_{10}(CO_3)_2$	40
29	$(Cu_{0.5}C_{0.5})Ba_2Ca_{n-1}Cu_nO_{2n+3}$	117 (n = 4)
30	$YCaBa_4Cu_5(NO_3)_{0.3}(CO_3)_{0.7}O_{11}$	82
31	$CuSr_{2-x}La_xYCu_2O_7$	60
32	$GaSr_2Ln_{1-x}Ca_xCu_2O_7$	73
33	$(C_{0.35}Cu_{0.65})$ $Sr_2(Y_{0.73}Ce_{0.27})_2Cu_2O_x$	18
34	$Bi_4Sr_4CaCu_3O_{14+x}$	84

n represents the number of CuO_2 layers in the compound (data from [8], with permission from R.P. Aloysius)

brings down the transition temperature. At stoichiometric O_7, copper exists in divalent and trivalent state as per the expression below:

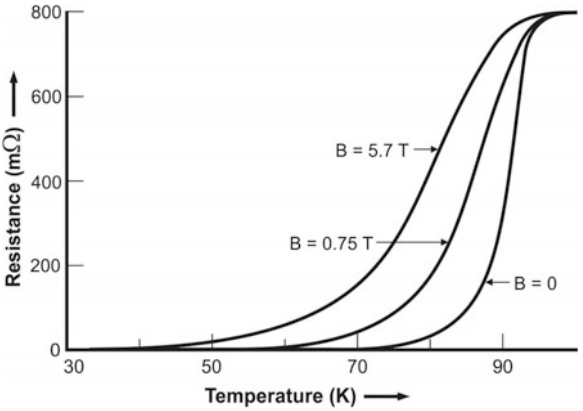

Fig. 4.4 Resistivity/temperature plot of Y–Ba–Cu–O at different magnetic fields by Wu et al. [9]. (With permission from APS) http://journals.aps.org/prl/abstract/10.1103/PhysRevLett.58.908

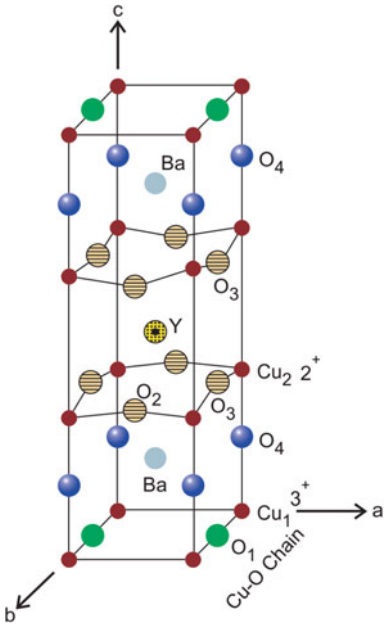

Fig. 4.5 Crystal structure of $Y_1Ba_2Cu_3O_7$. Notice two Cu–O sheets in the *a*–*b* plane sandwiching Y-atom and the Cu–O chains along the *b*-axis

$$\text{At } O_7 \qquad Y_1Ba_2Cu_3O_7 = Y^{3+}Ba_2^{2+}Cu^{3+}(1)Cu_2^{2+}(2)O_7^{2-} \tag{4.1}$$

Oxygen depletion leads to change in structure from orthorhombic to tetragonal. T_c starts decreasing with oxygen loss and so does the oxidation state of Cu. As O content decreases from 7 to 6.5, T_c decreases from 93 to 55 K and Cu(1) and Cu(2) are in divalent state. At $O = 6.5$ the material becomes semiconducting. In fact there is a plateau in the T_c versus O-content curve at $O_{6.5}$. As O-content decreases further, T_c decreases too and at $O = 6$, the material turns into an insulator. The oxidation

state of Cu reduces to univalent. The oxidation states of Cu at O_6 and $O_{6.5}$ can be expressed like this:

$$\text{At } O_{6.5} \qquad Y_1Ba_2Cu_3O_{6.5} = Y^{3+}Ba_2{}^{2+}Cu^{2+}(1)Cu_2{}^{2+}(2)O_{6.5}{}^{2-} \tag{4.2}$$

$$\text{At } O_6 \qquad Y_1Ba_2Cu_3O_6 = Y^{3+}Ba_2{}^{2+}Cu^{1+}(1)Cu_2{}^{2+}(2)O_6{}^{2-} \tag{4.3}$$

There is a striking correlation between the T_c and the oxidation state of Cu. T_c is found to be maximum when the oxidation state of Cu is $^{+}2.2$ which is found to correspond to O_7 stoichiometry. Both T_c and the copper oxidation state scales with the oxygen stoichiometry almost identically as seen from Fig. 4.6. T_c thus seems to be strongly dependent on the valence state of Cu which is controlled by the oxygen stoichiometry. One can explain this correlation between the valence state and T_c on the basis of the so-called charge transfer model. A detailed crystal structure of YBCO system, a repeat unit cell, is shown in Fig. 4.7. The CuO_2 planes sandwiching the Y-atom constitute the conduction layers. These double CuO_2 planes are separated by the so called charge reservoir or the intercalating layers which consists of metal-oxygen layers of Cu, Ba and oxygen. Many cuprate superconductors have been discovered by manipulating the number of CuO_2 planes, metal atoms in the charge reservoir layer and crystal structure. Quite a few of these cuprates are tabulated along with their T_c values in Table 4.2. YBCO has two Cu-atoms per unit cell in the conduction layer and one Cu-atom in charge transfer layer forming Cu–O chains. A reduction of O from 7 to 6 leads to equal distribution of O along the a and b-axes and the structure changes from orthorhombic to tetragonal. The tetragonal phase is not superconducting. Holes are created in the conduction layers as the electrons are transferred to charge reservoir layers. This changes the oxidation state of Cu to optimum value ($Cu^{+2.2}$) in the conduction layer causing the material to turn superconducting.

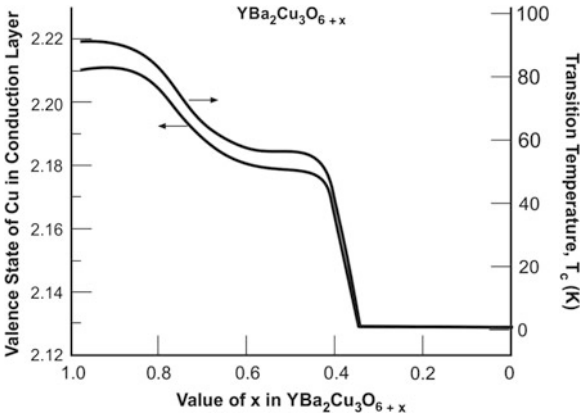

Fig. 4.6 T_c and the valence state of Cu in YBCO plotted against O-contents. T_c decreases as the oxygen content decreases from 7 to 6. Note the similarity in the two *curves*. Highest T_c occurs at $Cu^{+2.2}$ (from my lecture-notes, original data source could not be traced)

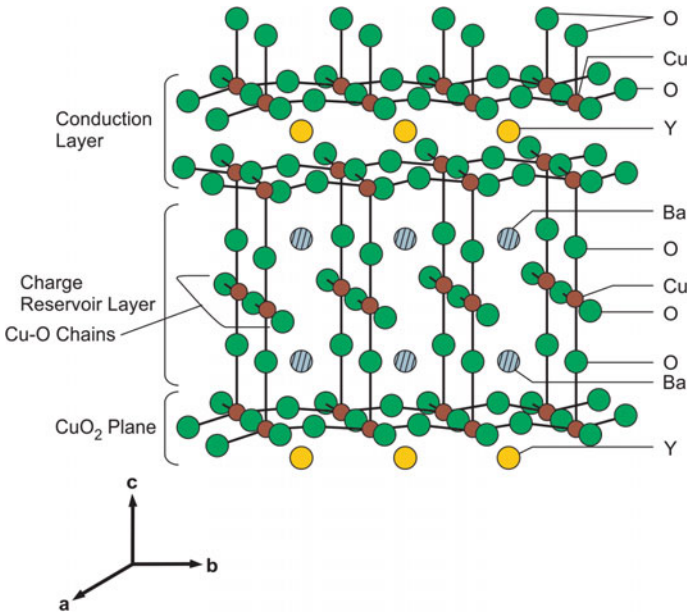

Fig. 4.7 A repeat unit cell structure of $Y_1Ba_2Cu_3O_{7-x}$. The CuO_2 planes on either side of Y-atom are the conduction layers and the Cu–O chains and the Ba–O planes constitute the charge reservoir layers

Even though YBCO remains to be the most studied and developed system, yet Y can be replaced by almost all the rare earth elements except Pr and Cs yielding this 123 compound with a T_c = 90 K. Even the magnetic material Gd yields Gd123 superconductor with T_c = 90 K.

4.2.1 Method of Synthesis of YBCO

The most popular technique for synthesizing Y123 is the standard technique of solid state diffusion [10]. Appropriate quantities of Y_2O_3, $BaCO_3$ and CuO, as per the formula unit $Y_1Ba_2Cu_3O_{7-x}$ are mixed thoroughly and ground in a pestle mortar. The fine powder so prepared is calcined at around 900 °C for about 20 h. This powder is finely crushed and calcined again. This process is repeated about three times when a homogenous mixture is obtained. The powder is now pressed into the form of a pellet or a bar and sintered at 920 °C for 20–25 h under flowing oxygen. Pieces of desired dimensions can now be cut from this pellet for different types of measurements. It is important to cool the sample slowly from the sintering temperature to have the stoichiometric oxygen (O_7) in the compound. Our experience shows around 60 °C/h. cooling rate is optimum [11]. Fast cooling changes the orthogonal phase into the tetragonal phase and makes the material non

superconducting. Target pellets are also prepared for thin film deposition following this method. Adequate oxygen supply during the sintering process is essential to get oxygen stoichiometry to 7.0. This becomes rather difficult while supplying oxygen to Ag-clad wires. The author has used successfully an addition of HgO to the bulk YBCO before calcinations which provides an internal source of oxygen [12–14]. A perfect O_7 stoichiometry has been obtained using this technique.

4.2.2 Some Peculiar Properties of YBCO

These cuprate superconductors are highly anisotropic materials and have widely different characteristic parameters and properties in the *a-b* plane and along the *c*-axis. Amongst the family of cuprates YBCO is, however the least anisotropic. A well oxygenated stoichiometric YBCO superconductor, for example, has the following typical parameters (Table 4.3).

Another peculiar property observed in these cuprates was the linear variation of the normal state resistivity with temperature down to T_c. Even though normal metals have linear ρ–T at higher temperature ($\sim\theta_D$) and $\rho\ \alpha\ T^5$ at low temperatures. The linear ρ–T behaviour in these compounds cannot be explained on the basis of electron-phonon interaction since the mean free path ($\sim$100–200 Å) is much greater than the lattice parameter ($\sim$3.8 Å).

4.2.3 YBCO Wires and Tapes

High hopes were generated, first time, to use this material for high field superconducting magnets and operate them at 77 K but the results were disappointing. The critical current in bulk YBCO superconductor drops down sharply with the application of magnetic field for a variety of reasons. One important reason is that

Table 4.3 Typical parameters of a stoichiometric $Y_1Ba_2Cu_3O_7$ in the *a-b* plane and along the *c*-axis

Parameter	$Y_1Ba_2Cu_3O_7$
Critical temperature, T_c (K)	93 K
Lattice parameters	a = 3.8591 Å
	b = 3.9195 Å
	c = 11.8431 Å
Coherence length (0 K)	$\xi_{ab}(0)$ = 15 Å
	$\xi_c(0)$ = 3 Å
London penetration depth	$\lambda_{ab}(0)$ = 1,400 Å
	$\lambda_c(0)$ = 7,000 Å
Normal state resistivity	ρ_{ab} = 0.5 m Ω cm and metallic
	ρ_c = 20 m Ω cm and semiconducting

these materials happen to be grainulus [10, 15] with grain boundaries which are weakly superconducting or even insulating. High critical current densities have however been reported in epitaxially grown YBCO films [16] and in YBCO single crystals [17]. This resulted in high expectation of developing this material with high critical current densities needed for high field applications. The critical current within the grain has been found to be quite high $\sim 10^6$ A cm^{-2} at 77 K. After a few years of intensive research, the focus of R&D activity shifted from research laboratories to industry for their commercial production. American Superconductors, Furukawa, SuperPower and Sumitomo are some leading companies marketing HTS wires, tapes and current leads. 2G YBCO or rather 2G REBCO coated conductors are increasingly used for power devices like FCL (fault current limiter), transformer and rotating machine. The fabrication techniques employed to produce these materials will be discussed in Chap. 6 titled 'Practical Superconductors'.

4.3 The Bi–Sr–Ca–Cu–O (BSCCO) System

Soon after the discovery of superconductivity in YBCO system at 93 K, Maeda et al. [18] reported superconductivity above 100 K in a Bi–Sr–Ca–Cu–O system, first high T_c material without a rare earth element. Figure 4.8 shows the version of the original curve of the resistance versus temperature behaviour of this compound which happens to be a multi phase superconductor. This was the first observation made by Maeda's group on 24th Dec 1987. An onset of superconducting transition was observed at 114 K with a tendency to go to zero resistivity at 105 K. A second transition is observed showing zero resistivity at 80 K. Their initial attempts to isolate

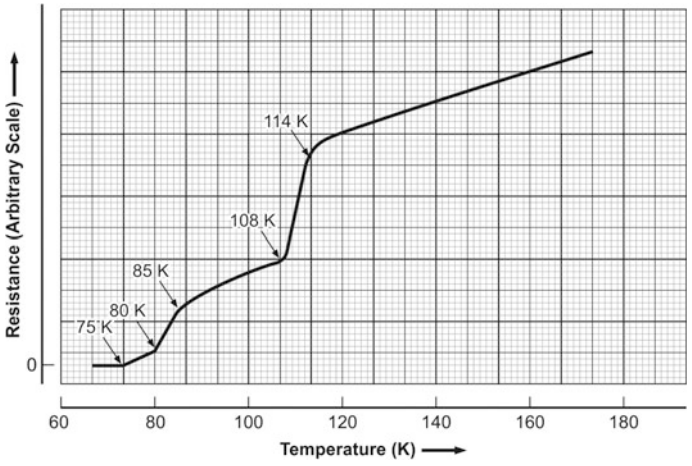

Fig. 4.8 Replicated original resistance versus temperature plot of Bi–Sr–Ca–Cu–O by Maeda et al. The *curve* shows multiple superconducting transitions at 114, 108 and 85 K [18]

the high T_c phase failed and they announced the discovery on Jan 21, 1988. Takano et al. [19] however succeeded in stabilizing the high T_c phase (=110 K) through the partial substitution of Bi by Pb. Further studies established the coexistence of three distinct crystallographic phases, namely the $Bi(Pb)_2Sr_2Ca_2Cu_3O_x$ phase, $Bi_2Sr_2Ca_1Cu_2O_y$ phase and $Bi_2Sr_2CuO_z$ or simply referred to as Bi-2223, Bi-2212, and Bi-2201 phases with T_c values of 110, 80 and 10 K respectively. In our laboratory we have been obtaining phase pure Bi-2223 material by solid state and also by solution technique with a T_c of 110 K. Best results have been obtained on nominal composition like $Bi_{1.6}Pb_{0.4}Sr_2Ca_{2.2}Cu_{3.5}O_y$ [20] and $Bi_{1.7}Pb_{0.4}Sr_{1.8}Ca_2Cu_{3.5}O_y$ [21] which are rich in Ca and Cu and deficient in Sr. These Bi-cuprates have orthorhombic structure, have Cu–O layers separated by Sr–O and Ca–O layers and two double Bi–O layers at the two ends of the unit cell. As seen from Fig. 4.9 the *c*-axis increases with the number of Cu–O layers. The *c*-axis is 24.6 Å for the 2201 phase, 30.89 Å for 2212 phase and 37.1 Å for the 2223 phase. There is one Cu–O layer in the 2201 phase, two Cu–O layers in 2212 phase and three Cu–O layers in the 2223 phase. It appears T_c goes up as the number of Cu–O layers increase. T_c has however been found decreasing if the number of layers increases beyond three. Crystals of Bi-cuprates have mica like morphology.

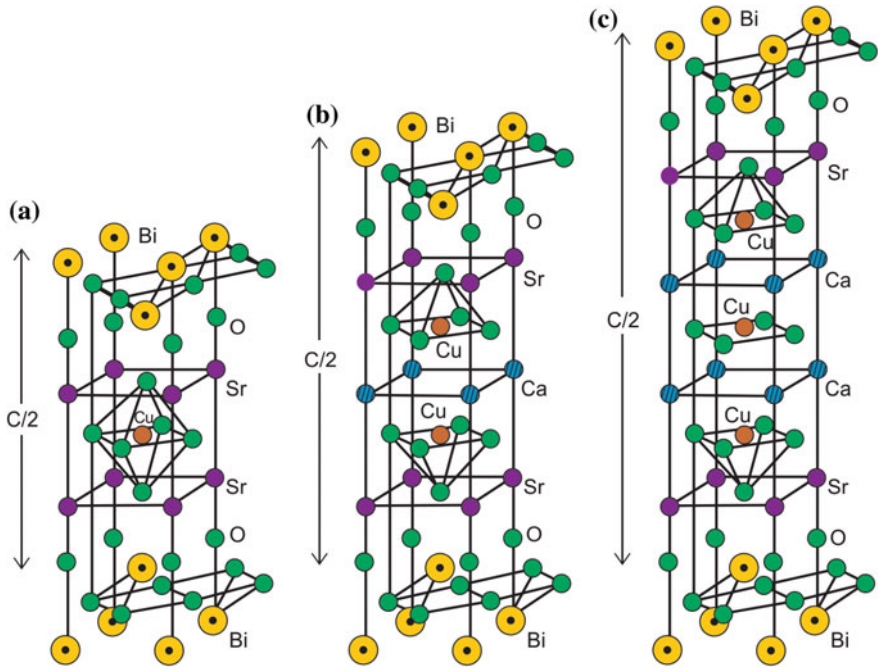

Fig. 4.9 The unit cells of the three Bi-compounds with compositions 2201, 2212 and 2223 having one, two and three Cu–O layers and increasing *c*-axis value respectively. **a** 2201 $Bi_2Sr_2Cu_1O_6$ (semiconductor phase) C = 24.6 Å, **b** 2212 $Bi_2Sr_2Ca_1Cu_2O_8$ (low T_c phase) C = 30.89 Å, **c** 2223 $Bi_2Sr_2Ca_2Cu_3O_{10}$ (high T_c phase) C = 37.1 Å

The 80 K Bi-2212 compound show modulation in the *ab* plane structure with 4b periodicity. The modulation is related to oxygen content and the Bi–O layers but does not play role in superconductivity. Inter-growth of the phases is a problem in the synthesis of Bi compounds. Some times this intergrowth has been found [21, 22] to provide effective flux pinning enhancing critical current density, J_c in Bi-2223 system.

4.3.1 Bi-2223 Wires and Tapes

Until the recent arrival of 2G, YBCO wires, Bi-2223 was the only material which has been commercially produced and used in applications like magnets, current leads high gradient magnetic separators, fault current limiters and the likes. Bi-2223 had been the favorite high T_c material for manufacturing because one needs to use a simple PIT technique followed by mechanical drawing, rolling and re-bundling with intermediate heat treatments. Typical cross section of a circular wire and a rectangular tape with multifilaments are shown in Fig. 4.10. Another more subtle reason is that the *c*-axis grain alignment can easily be achieved when shaped into the form of tapes. Grain alignment is achieved during the rolling process when compressive stress forces the plate like Bi-2223 grains to align parallel to the tape surface. Weak link problem is thus minimized in this material. Bi-2212 on the other hand needs heat treatment of the partially melted material followed by solidification after the tape forming to get the grain alignment. NRIM (now NIMS) together with Asahi Glass and Hitachi Cable Group in Japan produced a field of 21.8 T at 1.8 K by using a Bi-2212 coil [23] as the inner most insert. A back ground field of 18 T was provided by a combination of Nb–Ti and Nb_3Sn coils. The tapes were fabricated following the doctor-blade technique.

The problem with high T_c material is that the critical current density, J_c in these materials drops rather sharply in increased magnetic field when operated at high temperature, 77 K. This is primarily due to the weak pinning at these temperatures and the large anisotropy of J_c. Both are caused by the 2D nature of the structure of BSCCO system. The CuO_2 layers where the superconductivity resides, are separated by weakly superconducting or non superconducting oxide layers. When a

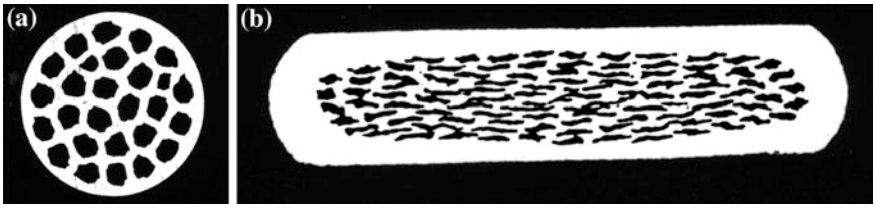

Fig. 4.10 Cross-section of the multifilamentary Ag/B(P)SCCO wires (**a**) and tapes (**b**) [8] (*Courtesy* R.P. Aloysius)

magnetic field is applied parallel to the layers (along the *ab*-plane), vortices pass through the weakly superconducting layers (charge transfer layers) but CuO_2 layers prevent the vortex movement in the perpendicular direction. This is the new type of pinning force called 'intrinsic pinning' [24]. BSCCO tapes in parallel field configuration can thus be used even at 77 K and still carry significant current. In field parallel to *c*-axis the vortex is divided into segments by non superconducting layers because of extremely small coherence length along this axis. This segment is referred to as 'pancake vortex' [25] and is confined within the CuO_2 layer and free to move because it is not strongly connected with the vortex in the next layer. In our initial studies on MF Ag/BSCCO tapes [21] we found a variety of impurity induced defects which probably served good pinning centres in a low purity commercial (CuO 99 %) grade material tapes. Figure 4.11a shows dislocation network in a (001) basal plane in a Ag/BSCCO-2223 tape with a core thickness of 140 μm. The same tape is further rolled to small thickness where the core thickness is reduced to 7 μm. As shown in Fig. 4.11b the dislocation density increases and improves the flux pinning. The dislocation network corresponds to the low-angle grain boundaries. The J_c value of the 7 μm (b) sample is 6.14×10^3 A cm^{-2} (77 K, self field) and 1.49×10^5 A cm^{-2} (4.2 K, self field). Yet another type of defect structure observed in the (b) sample is the intergrowth of the two phases viz; the low T_c (2212) and the high T_c (2223) phase with a *c*-axis parameters of 30.89 and 37.1 Å respectively. The J_c value after the rolling and re-sintering process is found to increase substantially. The commercial grade CuO (99 %) was found to have 60 ppm Fe which preferentially occupies the Cu(II) square pyramidal site as revealed by Mössbauer studies. This results in stacking faults and the intergrowth of the 2212 and 2223 phases (Fig. 4.12). These defects can be expected to provide effective flux pinning sites and raise J_c, as observed experimentally.

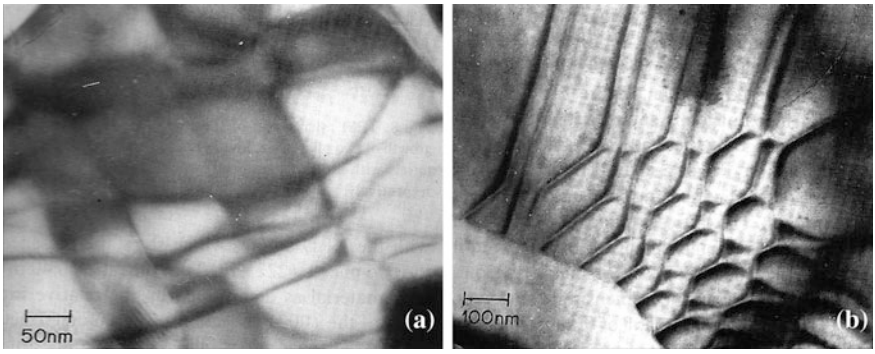

Fig. 4.11 Transmission Electron Micrographs of the core material of a Ag/BSCCO-2223 tape prepared using commercial grade oxides and carbonates. **a** is a tape with 140 μm thick core and shows dislocation network in (001) basal plane. **b** is the same tape rolled down to a core thickness of 7 μm and re-sintered. The density of dislocation increases in (**b**) sample. The dislocation network corresponds to the low angle twist grain boundaries. J_c too increases [21] (With permission from Elsevier)

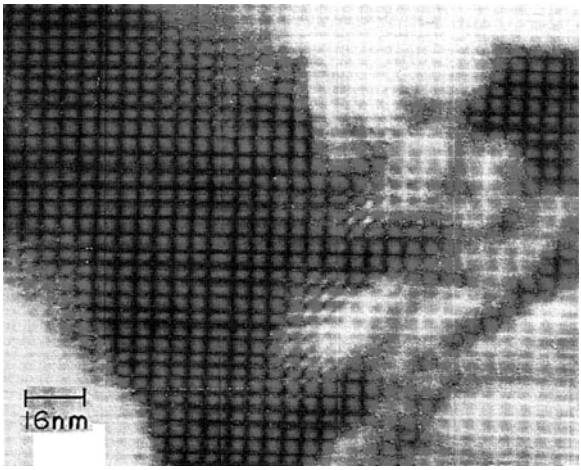

Fig. 4.12 TEM micrograph of (**b**) sample of Ag/BSCCO-2223 tape, rolled to fine size (7 μm core) and re-sintered which shows the intergrowth of low T_c (2212) and high T_c (2223) phases [21] (With permission from Elsevier)

Among several manufacturers of the Ag/BSCCO wire, American Superconductors (AMSC) of USA and Sumitomo Electric Company (SEC) of Japan were the main players supplying this material for different applications. AMSC mainly supplied two types of wires. One code named 1G-HSP HTS (high strength plus HTS wire) meant for applications where high mechanical strength was required. This wire had BSCCO-based multifilaments (MF) and was encased in a Ag-alloy matrix with a SS lamination. Typically, the wire thickness was 0.26 mm, width 4.2 mm and a room temperature maximum tensile stress of 200 MPa which goes up to 250 MPa at 77 K. The wire had a maximum tensile strain of 0.4 % and an engineering current density, J_c of 13.3×10^3 A cm^{-2} (77 K and self field). The second type of MF BSCCO wire with high current density too was encased in a Ag-alloy matrix. This wire was 0.22 mm thick, 4.0 mm wide, had a maximum RT tensile strength of 65 MPa and a maximum tensile strain of 0.1 %. Maximum I_c was 155 A which corresponds to a $J_c = 17.2 \times 10^3$ A cm^{-2} (77 K and self field). The wire length available was 800 m. AMSC has now stopped producing this material and has switched over to 2G YBCO wires already discussed in Sect. 4.2.3. The BSCCO conductor now receded to background is now referred to as G-1 (first generation) high T_c superconductor. We will present the present status of 2G REBCO conductors in Chap. 6 on "Practical Superconductors".

SEC of Japan had been marketing Ag-matrix clad BSCCO wires in 2 km lengths under the code name DI-BSCCO wires [26]. DI here means Dramatically Innovative CT-OP (controlled over pressure sintering) process. Sintering is carried out under a gas pressure (partially oxygen) of 30 MPa. The wire has an excellent J_c behaviour up to a field of 10 T. The wire carries an I_c of 218 A (1 mm^2). The wires are laminated with either SS or brass as per the strength requirement. Wires with 50 μm SS lamination can withstand a stress of 400 MPa.

4.3.2 First Generation (1G)-BSCCO Current Leads

One most popular use of HTS had been in current leads employed in superconducting magnets both bath-cooled and conduction-cooled. The (1G) BSCCO current leads capable of transporting current in excess of 3,000 A have been commercially marketed for decades now. 'Can Superconductors' of Czech Republic, American Superconductors of USA and Bruker Energy and Supercon Technologies are some of the suppliers of these current leads. Current leads are generally used to transport current from 77 K thermal shield to magnet maintained at $\sim$4 K with no Joule heating. Moreover, the thermal conduction through the leads too is poor which makes the magnet system energy efficient. Current carrying capacity almost doubles if the higher temperature end is kept at around 64 K instead of 77 K. Typically, a current lead with I_c = 1,500 A between 77 and 4 K has a conductive heat leak of 0.6 W, whereas if used between 64 and 4 K the heat leak reduces to only 0.4 W. Current leads can be bulk tube type or encased for protection (Fig. 4.13). Copper studs or copper braids are provided for jointing/soldering purpose. Figure 4.14 is a 100 A pair of BSCCO-2223 current leads developed [8] by the NIIT, Trivandrum. The development of BSCCO current leads made it possible to build cryo-free superconducting magnets which found popularity in low temperature laboratories in last two decades. The reduction in heat generation in the current leads had been so significant that a closed cycle refrigerator (CCR) with a cooling capacity of 1.5 W can cool a large size magnets to $\sim$3 K in a reasonable time of few hours. Chap. 7 will discuss the construction of such a cryo-free magnet with a special reference to a 6 T room temperature bore magnet built in author's laboratory using a 1.5 W CCR of Sumitomo make some years ago.

Fig. 4.13 Bulk and encased current leads marketed by M/S 'Can Superconductors' and used in author's lab (IUAC Delhi)

Fig. 4.14 A pair of 100 A, BSCCO-2223 current leads developed by NIIST, Trivandrum. Leads with higher current rating available [8] (*Courtesy* R.P. Aloysius)

4.4 The Tl–Ba–Ca–Cu–O System

The race to discover still higher T_c superconductors continued and yet one more cuprate superconductor of the type Tl–Ba–Ca–Cu–O with T_c of greater than 90 K was discovered by Sheng and Hermann [27] in 1988 itself. The zero resistivity in this compound was obtained at 81 K. Soon a T_c of 120 K was reported by the same authors [28] in a compound $Tl_{1.86}CaBaCu_3O_{7.5+y}$. This was the highest T_c cuprate without a rare earth constituent. Since Tl_2O_3, the ingredient of the compound has a low melting point of 717 °C and starts decomposing at 100 °C, the preparation method for this compound is different. Sheng and Hermann have followed a 'short high temperature and quenching technique'. Appropriate amounts of $BaCO_3$ and CuO were mixed, ground and heated to 925 °C for >24 h in air with several intermediate grindings. Black compound like $BaCu_3O_4$ or $Ba_2Cu_3O_5$ are formed during this process. Right amount of Tl_2O_3 was then added, pressed into a pellet and kept in a tubular furnace already heated to about 900 °C under flowing oxygen. The pellet was kept for 2–5 min and quenched in air to room temperature and used for studies.

Still higher T_c of 125 K was reported [29] in quick succession in the same compound with stoichiometry $Tl_2Ca_2Ba_2Cu_3O_x$ (Tl-2223) quite analogous to Bi-2223 compound. The unit cell of this compound is bcc tetragonal containing three Cu perovskite like units separated by bilayers of TlO. T_c ranges between 118 and 125 K depending on the preparation parameters. Another compound with composition $Tl_2Ba_2Ca_1Cu_2O_x$(2212) is a bulk superconductor with T_c = 95–108 K. This compound has two Cu perovskite units similar to Bi-2212 compound.

Figure 4.15 shows how T_c increases with the number of CuO layers from one to three. Tl compounds can be expressed with the general formula $Tl_2Ba_2Ca_{n-1}Cu_nO_{2n+4}$ and are tetragonal with two Tl–O layers and n Cu–O layers. T_c values are 80, 110 and 125 K for three compounds with n = 1, 2 and 3 respectively. T_c is found increasing with the increase of Cu–O layers only up to n = 3. T_c decreases for n > 3. Tl being a toxic material, no attempts have been made to produce this material either on a laboratory scale or on a commercial scale for applications.

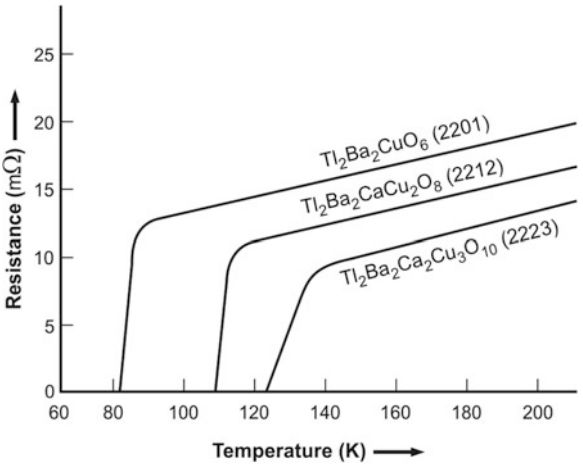

Fig. 4.15 Superconducting transition in three compositions of Tl compounds viz; 2201, 2212 and 2223. T_c increases with the number of Cu perovskite units 1, 2 and 3 respectively

4.5 The Hg–Ba–Ca–Cu–O System

After a lull of about 5 years, once again a new superconductor was discovered with T_c of 94 K by Putillin et al. [30] in a compound, $HgBa_2CuO_{4+y}$ or simply called Hg-1201 (as Ca is absent). This is very high T_c in contrast to the similar Tl-1201 compound which has a T_c of <10 K. This compound has one Cu–O_2 sheet. Mercury compounds can in general be described by a formula of the type $HgBa_2Ca_{n-1}Cu_nO_{2n+2+y}$ where n can take different values starting from 1 onwards. Soon superconductivity was discovered at 130 K by Schilling et al. [31] in a multiphase Hg-compound with $n = 1, 2$ and 3. Soon the pure phase $HgBa_2Ca_2Cu_3O_{8+\delta}$ was synthesized with $n = 3$ and a $T_c = 135$ K was obtained. The unit cell structure of the three Hg-compounds with $n = 1$, 2 and 3 are shown in Fig. 4.16. Evidently *c*-axis increases with the number of CuO_2 layers. Analogous to Tl-system Hg-system too has a tetragonal structure with '*a*' and '*c*' parameters as given in the figure. An enhancement in T_c with pressure in copper containing superconductors with hole conductivity is well known. Chu et al. [32] reported a T_c of 153 K for the compound $HgBa_2Ca_2Cu_3O_{8+\delta}$(1223) at a pressure of 150 kbar. In a systematic study Gao et al. [33] found continuous increase in T_c of all the Hg-compound(1201, 1212 and 1223) up to a pressure of 45 GPa, viz; 164 K for 1223, 154 K for 1212 and 118 K for the compound 1201. T_c values with increasing pressure for Hg-compounds with $N = 1, 2, 3$ and 4 are plotted in Fig. 4.17 [34]. In all the compounds T_c increases with pressure and tend to saturate at high pressure. It has been conjectured that it may be possible to get T_c values as high as 164 K under ambient pressure in optimally doped compounds through substitution if the Cu–O distances can stabilize.

Synthesis of Hg-compound is little complicated because of the toxicity of Hg and decomposition of HgO into Hg and oxygen at comparative low temperature

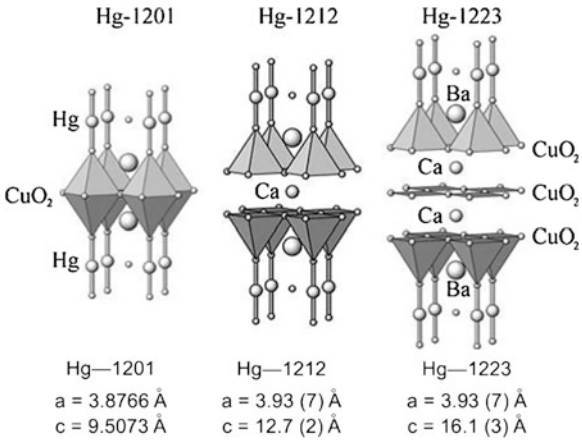

Fig. 4.16 Unit cell structure of $HgBa_2CuO_{4+\delta}$(1201), $HgBa_2Ca_1Cu_2O_{6+\delta}$(1212) and $HgBa_2Ca_2Cu_3O_{8+\delta}$(1223) with one, two and three CuO_2 layers respectively [34] (With permission from IOP)

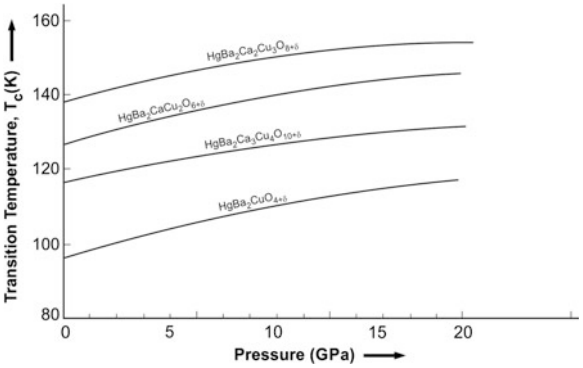

Fig. 4.17 T_c increases with pressure for Hg-compounds and with the number of CuO_2 layers up to $n = 3$. T_c decreases with pressure for compound Hg-1234 ($n = 4$). T_c is thus highest for Hg-1223 ($n = 3$) [34] (With permission from IOP)

(430 °C). Samples are prepared in sealed quartz ampoules, and of either platinum or gold containers to prevent reaction. The synthesis is a two-step process. In the first step stoichiometric mixture of barium carbonate (oxalate, nitrate or oxide), copper and calcium oxides is prepared and annealed at 600–1,000 °C in air, Oxygen flow or vacuum. The precursor so prepared is extremely hydroscopic and absorb CO_2 fast. All the operations are therefore carried out in a dry box. HgO is then added to the mixture and sealed in an ampoule for further annealing. T_c of these compounds has been found extremely sensitive to the presence of carbon and steps should therefore be taken to avoid carbon contents in the starting materials. An excellent topical review on the structure and synthesis of Hg-compounds has been written by Antipov et al. [34] on Hg-compounds. As far as the commercial production of

cuprates is concerned, Bi-2223 had been the most favoured materials for magnet based applications and the current leads until recently. Hg-compound wires and tapes have not been exploited for commercial production or applications.

4.6 Discovery of Superconductivity in Magnesium Diboride (MgB_2)

Nature surprised us yet again when Nagamatsu et al. [35] reported the discovery of superconductivity at 39 K in magnesium diboride, MgB_2 outside the cuprate family. This material had been known to us since early 1950s but not as a superconductor. Figure 4.18a shows the original magnetic susceptibility versus temperature curves for MgB_2 by Nagamatsu et al. [35] under zero-field cooled (ZFC) and field cooled (FC) conditions. Figure 4.18b on the other hand shows the electrical resistivity behaviour with temperature. Both the measurements give a sharp superconducting transition at 39 K. In fact, interest had been growing to look for superconductivity in intermetallic compounds with light elements like boron since 1994 when superconductivity was discovered in borocarbides [36, 37] These materials are of the type RE-Tm_2B_2C where RE is a rare earth such as Y, Lu, Er, Dy, Tm is Ni or Pd. The study of these materials had been of interest because of high T_c observed among the intermetallics (e.g. T_c = 23 K in YPd_2C), the unique anisotropic layered structure and an interplay between superconductivity and magnetism.

Excitement to exploit MgB_2 for applications grew for a variety of reasons. It is a cheap material compared to HTS cuprates where Ag constitutes almost 70 %, it has low anisotropy in its superconducting properties and T_c is in the range when one can operate MgB_2-based systems using close cycle refrigerators thus doing away with the use of liquid helium. We will therefore discuss this material a little more in

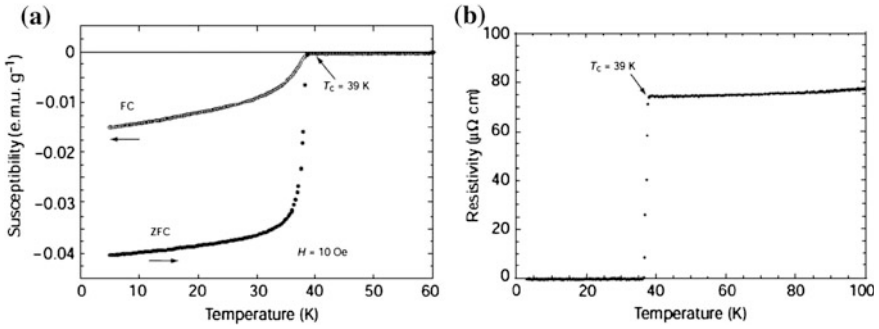

Fig. 4.18 **a** Magnetic susceptibility of MgB_2 under zero field (ZFC) and field cooled (FC) conditions plotted against temperature, **b** The electrical resistivity variation with temperature of MgB_2 both the measurements show a sharp superconducting transition at 39 K [35] (With permission from Nature Publishing Group)

detail. Search for similar diborides with comparable T_c turned out to be futile. Superconductivity was indeed found in niobium diborides (NbB_2) but with T_c (0.62 K), disappointingly low.

4.6.1 The Crystal Structure and the Origin of Superconductivity in MgB_2

MgB_2 is metallic and has a layered hexagonal structure [38]. The B atoms form a graphite like honeycombed layers and the magnesium atoms occupy the centre of the hexagons in between the boron planes as shown in Fig. 4.19. MgB_2 is quite similar to conventional metallic superconductors except that it has high T_c, remains metallic all through unlike the cuprates which are insulator without doping. It has nevertheless one dissimilarity with them in so far as MgB_2 is characterized by two energy gaps. This indicates that it has two different species of electrons with different kinds of bonding forming pairs and leading to superconductivity. Choi et al. [38] for the first time carried out calculations from the first principle and obtained numerical values of the two energy gaps and their effects on the measurable parameters. These authors have been able to account for the high T_c, the anomalous specific heat versus temperature behaviour and for the isotopic substitution. The observed isotope effect also led them to believe that the pairing is mediated via the

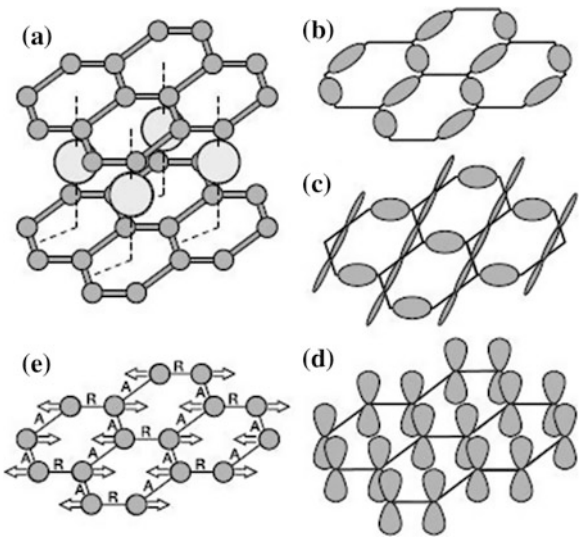

Fig. 4.19 Crystal structure of MgB_2 [38]. **a** The crystal structure of MgB_2, **b**, **c** σ-bonding states of the Fermi level derived from boron p_{xy} orbitals, **d** a π-bonding state of the Fermi level derived from boron p_z orbitals, **e** a vibrational mode of boron atoms that couples to σ-bonding electronic states at the Fermi level (With permission from Nature Publishing Group)

lattice vibrations and the superconductor is of BCS type. An important feature of their analysis is that the electronic states formed by the orbitals in the boron plane interact strongly with the specific phonon modes leading to pair formation and the superconductivity.

The authors have used Eliasberg approach of strong coupling superconductivity based upon the BCS theory. Their argument is that the electronic states at the Fermi level are mainly either σ or π-bonding boron orbitals. σ-bonding states resides within the boron planes. The σ-bonding states couple rather strongly with the in-plane vibrations of the boron atoms. This coupling leads to strong electron-pair formation of the σ-bonding states resulting in the appearance of an average energy gap of 6.8 MeV. This strong pairing in the boron planes, occupying the Fermi surface only partially is believed to be the main source of superconductivity. π-bonding states residing on the remaining part of the Fermi surface, on the other hand, form much weaker pairs with an average energy gap of 1.8 MeV. This pairing too can become stronger by coupling with the σ-bonding states. These average values of two energy gaps are found to be consistent with the experimental values. The calculated energy gaps-temperature variation is plotted in Fig. 4.20. As seen in the figure the large energy gap corresponding to σ-bonding states drops with the increase of temperature and quite fast close to T_c as compared to the smaller energy gap for the π-bonding states. Both the energy gaps merge and vanish at T_c, despite having very different values at low temperature.

The experimental energy gap parameters fit well with the calculated values and follow a temperature variation given by the equation of the type:

$$\delta(T) = \delta(0)[1 - (T/T_c)^p]^{\frac{1}{2}} \tag{4.4}$$

where $p = 2.9$ for the larger gap for the σ-bonding states and $p = 1.8$ for the smaller gap for the π-bonding states. This temperature dependence of the energy gaps has been verified by experimental data on tunneling, optical and specific heat

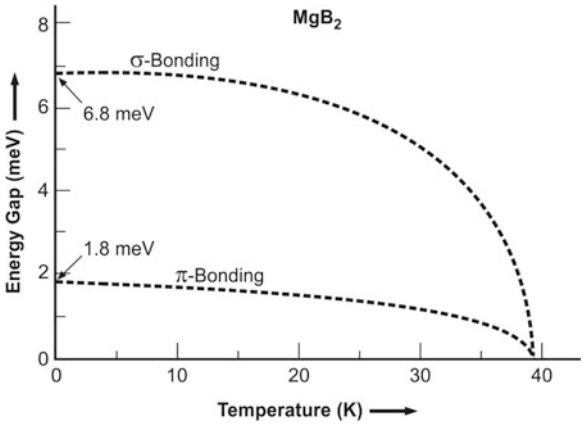

Fig. 4.20 The calculated average superconducting energy gap parameters plotted against temperature. Both the gaps merge and become zero at T_c [38] (With permission from Nature Publishing Group)

measurements. There is overwhelming evidence that MgB_2 is a BCS type superconductor with an intermediate to strong s-wave coupling. The existence of pairs with charge 2 e too has been established through ac and dc Josephson effect [39] studied on break junctions of MgB_2. Extensive studies have been carried out on almost all aspects of this material and a very large number of papers have been published. A few comprehensive reviews [40–42] have already been published on MgB_2 system. Nevertheless, we review in next section some important properties and related studies carried out on MgB_2.

4.6.2 A Summery of Studies on MgB_2

4.6.2.1 Preparation of Bulk MgB_2 and Fabrication of Wires/Tapes

Magnesium diboride is commercially available from chemical suppliers but the purity has to be ascertained. In the laboratory MgB_2 has been synthesized in various forms such as polycrystalline bulk, single crystal, thin film, wires and tapes following different techniques. Nagamatsu et al. [35] had prepared the first MgB_2 sample by the solid state reaction method. Appropriate quantities of Mg and B in the ratio 2:1 were mixed, ground and pressed in pallet form. The pellet was heated to 973 K under 196 MPa argon pressure using a hot isostatic pressing furnace for 10 h. The material can also be synthesized under ambient in an inert atmosphere. One can prepare bulk MgB_2 in a sealed ampoule to prevent the loss of Mg because of its volatile nature. Single crystals of the size $1.5 \times 0.9 \times 0.2$ mm^3 and weighing up to 230 μg have been grown [43] at high pressure through the peritectic decomposition of MgB_2. The single crystals have a T_c in the range of 37–39 K.

Methods followed to deposit MgB_2 film, are co-evaporation, pulse laser deposition (PLD), magnetron sputtering, deposition from suspension and Mg diffusion. Films have been deposited on a variety of substrates such as, SiC, Si, $LaAlO_3$, $SrTiO_3$, MgO, Al_2O_3 and SS. The choice of substrate is thus very wide because perhaps the hexagonal structure of MgB_2 can grow on a variety of substrates with different lattice parameters. The volatility of Mg has to be kept in mind. Target for sputtering therefore has to be kept Mg rich. Bulk MgB_2 is also prepared in a sealed ampoules for the same reason. Mg-diffusion technique (diffusion of Mg in B) has proved to be the best technique, be it bulk, films or wires.

For magnet coils we need superconducting material in the form of stabilized multifilamentary wire or a tape. Two methods are available to prepare the material in this form. One is the coating technique and the other PIT (powder-in-tube) technique. In the first technique, a moving ribbon mostly hastelloy is coated with MgB_2. Komori et al. [44] prepared MgB_2 tapes on hastelloy with a $J_c = 1.1 \times 10^5$ A/cm^2 at 4.2 K and 10 T field. H_{c2} as high as 55 T and an irreversible field of 40 T has been reported by Ferrando et al. [45] in a carbon alloyed MgB_2 coated conductor by a hybrid physical-chemical vapour deposition technique.

The coating technique discussed above though provides tapes with superior quality, nevertheless is not an ideal technique to produce long lengths (several km). PIT is a viable and preferred technique for commercial production. In this technique well prepared fine powder is packed at a high density in a metal tube and rolled/drawn to fine size of wires or tapes in a series of steps of rolling and intermediate annealing to maintain ductility. The sheath material should be such that it does not react with the core material and provides sufficient mechanical strength to the composite wire/tape. Copper has to be incorporated some how in the cross section of the wire/tape to provide thermal stability to the superconductor. Several metals such as Fe, Mo, Nb, Ta, Hf, W, Cu, Ag, Cu–Ni and SS have been used for cladding with varying degree of performance. The starting core material can be either preformed MgB_2 or a mixture of Mg and B in right proportion. In the later case a heat reaction at 900–1,000 °C is required so as to form stoichiometric MgB_2 core. High temperature treatment is not needed [46] in the case of preformed MgB_2. Stoichiometry, however, improves with heat treatment after the drawing process. Kumakura et al. [47] reported $J_c = 10^4$ A cm^{-2} at 4.2 K and 5 T values in a single core and a 7-core MgB_2 tapes fabricated using PIT technique with SS and Cu–Ni sheath material (Fig. 4.21). No heat treatment was carried out. The higher value of J_c for SS sheathed tape is achieved because of the higher packing density attainable. SS also provides higher mechanical strength. Feng et al. [48] prepared 1 mm dia. wires by PIT technique using 1020 Fe-sheath and following a wind and react method. Annealing was done under Ar atmosphere at a temperature of 850 °C for 30 min. They report a J_c value of 1×10^4 A cm^{-2} (4.2 K, 6 T) and 1.8×10^5 A cm^{-2} (20 K, 0 T). Fe, Ni and SS turn out

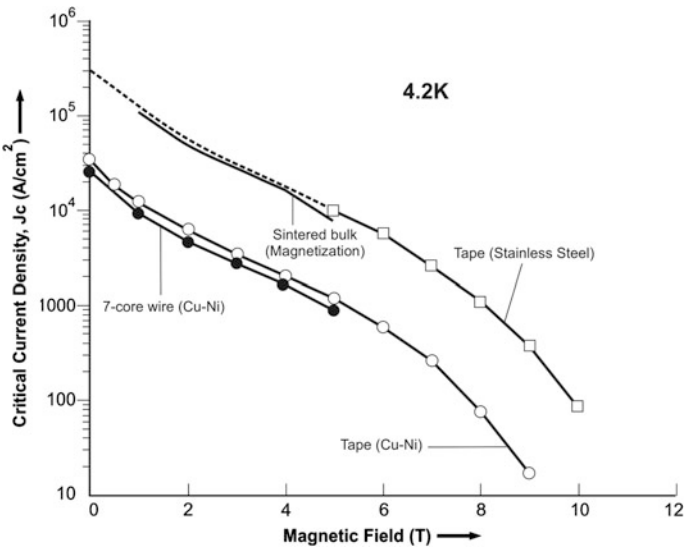

Fig. 4.21 Transport J_c versus magnetic field plots for Cu–Ni sheathed mono-core tape and Cu–Ni sheathed 7-core wire and SS sheathed mono-core tape at 4.2 K [47]. Reproduced with permission AIP Publishing LLC

to be the most suitable cladding materials. Copper has to be used with Nb or Ta barrier for thermal stability.

Sumption et al. [49] developed 7, 19 and 37 filament MgB_2 wires following the ex situ route. In some sample 30 μm size particles and in some samples excess Mg was incorporated. Single step heat treatment at 700–800 °C for 10–30 min was given. All the wires used either Nb or Fe as filament barrier. Filament size ranges between 80 and 150 μm. A $J_c = 1.75 \times 10^5$ A cm^{-2} (4.2 K, 5 T) has been achieved. At 20 K the intrinsic J_c appears to be reaching 10^6 A cm^{-2}. All these studies auger well for the potential application of MgB_2 superconducting wires for magnets operating with close cycle refrigerators.

4.6.2.2 Some Physical Properties of MgB_2

We briefly describe some physical properties and interesting studies that have been carried out on this material.

The Hall effect measurements [50] on MgB_2 single crystal reveal that it has two types of charge carriers, holes in the plane and electrons along the *c*-axis. There is anisotropy in electrical resistivity along the plane and in the perpendicular direction which turns out $\rho_c/\rho_{ab} = 3.5$. Normal state Hall coefficient is positive in plane (*B*//*c*, *I*//*ab*) and negative in the out-of-plane (*B*//*ab*, *I*//*c*) confirming that the electronic structure of MgB_2 is multi-band.

MgB_2 shows isotope effect quite convincingly confirming the phonon mediated Cooper pair formation in this material. Bud'ko et al. [51] through magnetization and specific heat measurements find a shift of T_c by 1 K in $Mg^{11}B$ and $Mg^{10}B$ prepared with two isotopes of B. The T_c values obtained are 39.2 and 40.2 K for the two intermetallics respectively. Conventional BCS superconductors follow the relation $T_c\ \alpha\ M^{-\alpha}$ where the isotopic exponent, α turns out to be 0.5. The value of boron isotope exponent α_B for MgB_2, however, comes out to be = 0.26 ± 0.03. This value of the exponent is very close to the values reported for YNi_2B_2C and $LuNi_2B_2C$ borocarbides. Mg does not display significant isotope shift in T_c and the isotope exponent for Mg is though non-zero but very small. This indicates that the phonons mediating for the occurrence of superconductivity are boron like. Some theories do hint at the possibility that the phonons responsible for superconductivity are high frequency boron A1 g optical modes.

Pressure is another important parameter which has been exploited to study this material. Lorenz et al. [52] have made detailed studies on ac susceptibility and Seeback coefficient with increasing pressure up to 1.84 GPa. T_c always decreases with increasing pressure and is linear with pressure. As shown in Fig. 4.22 T_c drops down with the increase of pressure till the highest pressure of 1.84 GPa. This drop in T_c is rather fast at a rate of −1.6 K/GPa and is close to the theoretically calculated value of −1.4 K/GPa. The Seeback coefficient has been found to be positive and relatively small. It decreases with the decrease of temperature similar to a metal with hole-type carriers.

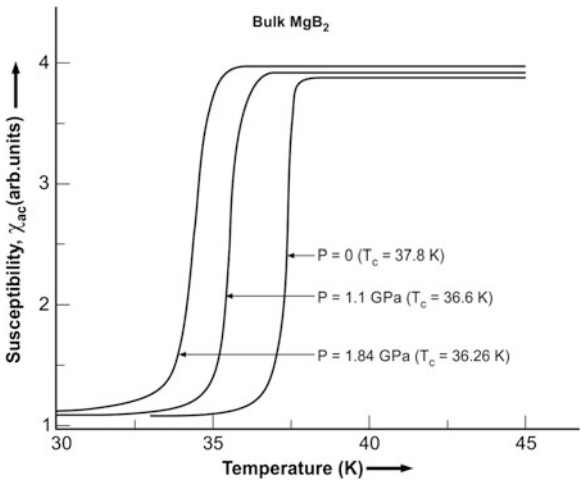

Fig. 4.22 Plots of ac susceptibility of bulk MgB_2 against temperature with increasing pressure up to 1.84 GPa. T_c shifts to lower temperature with increasing pressure [52]. (With permission from APS) http://journals.aps.org/prb/abstract/10.1103/PhysRevB.64.012507

Substitution at Mg as well as B sites with a host of elements always resulted in the decrease of T_c. Some of the materials tried are C, Al, Li, Si, Be, Cu, Mn, Nb, Ti, Fe, Co, Ni, and Zn. Decrease in T_c is severe in case of substitution with Mn, Co and C and slow with Si and Li. Least decrease in T_c occurs with Zn substitution

The coherence length values, as calculated from B_{c2}, range between 6.1 and 6.5 nm in *ab*-plane and between 2.5 and 3.7 nm along the *c*-axis. The most accurate data for a single crystal gives $\xi_{ab}(0)$ = 6.1–6.5 nm and $\xi_c(0)$ = 2.5–3.7 nm.

The penetration depth as evaluated from B_{c1} values range between 85 and 203 nm.

The lower critical magnetic field as reported by several investigators range from 25 to 48 mT.

Upper critical magnetic field B_{c2} has been reported for material in different forms like bulk, single crystal and thin films and in different orientations over a wide range of values ranging from 2.5 to 32 T. The highest value of B_{c2}, 32 T has been reported for films with T_c = 39 K. Higher B_{c2} = 40 T has been reported by Patnaik et al. [53] for films with lower T_c. B_{c2} drops almost linearly with increasing temperature saturating at low temperature. The B_{c2} anisotropy ratio = $\frac{B_{c2}^{ab}}{B_{c2}^{c}}$ = 1.1–1.7 is reported for textured bulk and partially oriented crystallites. Higher ratio = 1.8–2.0 has been reported [53] for *c*-axis oriented MgB_2 film. The irreversible field extrapolated to 0 K, range from 6 to 12 T for MgB_2 in bulk, thin film, powder, tape and wire. B_{irr} thus is =0.5 B_{c2} in MgB_2 instead of =0.8 B_{c2} for conventional low temperature superconductors. Impurity additions are known to increases the B_{c2} in type II superconductors as the mean free path is reduced and so does the coherence length $\xi(0)$. Braccini et al. [54] do report significant enhancement of B_{c2} in C-alloyed MgB_2 films irradiated with He-ions. The disorder thus introduced, raises in-plane B_{c2} to 51 T (4.2 K) and along the *c*-axis to 35 T (4.2 K). These are very promising values and show the potentiality of use of this material with high J_c in

Table 4.4 Some important superconducting parameters of MgB_2 (data compiled from references cited in the text)

Parameter	Unit	Value
Transition temperature, T_c	K	39
Penetration depth	nm	85–203
Coherence length, ξ_{ab}	nm	6.1–6.5
Coherence length, ξ_c	nm	2.5–3.7
Coherence length, ξ_{ab} single crystal	nm	6.1–6.5
Coherence length, $\xi_c(0)$ single crystal	nm	2.5–3.7
Lower critical field, B_{c1}	mT	25–48
Highest upper critical field (film)	T	32–40
$\frac{B_{c2}^{ab}}{B_{c2}^{c}}$ anisotropy (textured bulk/partially oriented crystellites)		1.1–1.7
$\frac{B_{c2}^{ab}}{B_{c2}^{c}}$ anisotropy (c-axis oriented films)		1.8
Irreversible field, B_{irr} (0 K)	T	6–12
Estimated paramagnetic limited field, H_{c2}^{ab}	T	70

high magnetic field. Extrapolation of data to $T = 0$ K shows that H_{c2}^{ab} might lead to paramagnetic limit of 70 T. Table 4.4 summarizes most of the important superconducting parameters of MgB_2.

4.7 The Discovery of Iron Based Superconductors

4.7.1 The LaFeAsO(1111) Compounds

One more surprise came from the Japanese group headed by Hideo Hosano [55] when they reported superconductivity in a new class of materials, the iron-based oxy-pnictides, of the type LaOFeP. The material has a tetragonal structure consisting of alternate layers of lanthanum oxide ($La^{3+}O^{2-}$) and iron pnictide ($Fe^{2+}P^{3-}$). The material had an on-set of T_c at 5 K and complete disappearance of resistivity at 3.2 K. The two dimensional ($Fe^{2+}P^{3-}$) layer is believed to be the conduction layer in which the charge carriers travel. Doping of the ($La^{3+}O^{2-}$) layer causes the transfer of carriers to the conduction layer. Replacing O^{2-} with F^- will provide a positive charge to the insulating La_2O_2 layer and a negative charge to the Fe_2As_2 conduction layer. This will lead to the strong electron interaction and modulation of the interaction through the density of state. T_c was found to increase with fluorine-doping. Soon the group reported [56] a high T_c of 26 K in iron-based $La(O_{1-x}F_x)FeAs$ layered superconductor. Here x varies from 5 to 12 %. The crystal structure of this superconductor is shown in (Fig. 4.23). The conduction layers Fe_2As_2 are sandwiched between the insulating La_2O_2 layers. It has a tetragonal structure of the type (ZrCuSiAs) with p4/nmm space group. The room temperature lattice parameters of

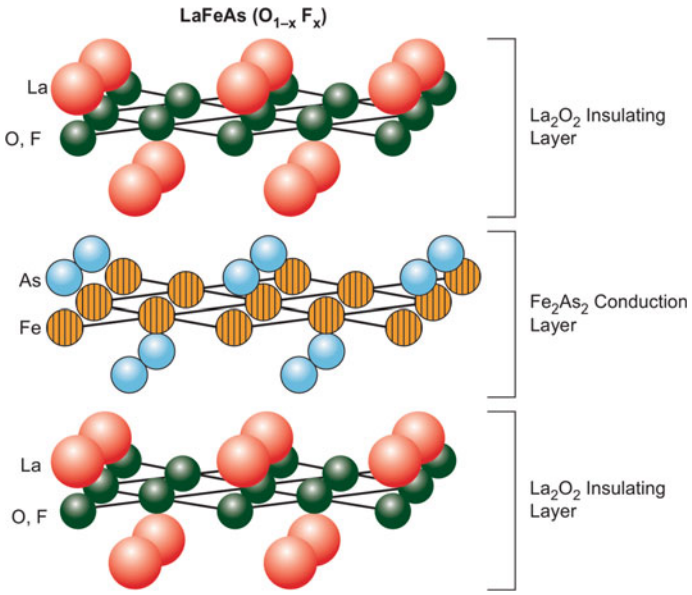

Fig. 4.23 The crystal structure of LaFeAsO system. The Fe_2As_2 conduction layers are sandwiched between the insulating La_2O_2 layers. The structure is of the type (ZrCuSiAs) [56] (With permission from American Chemical Society)

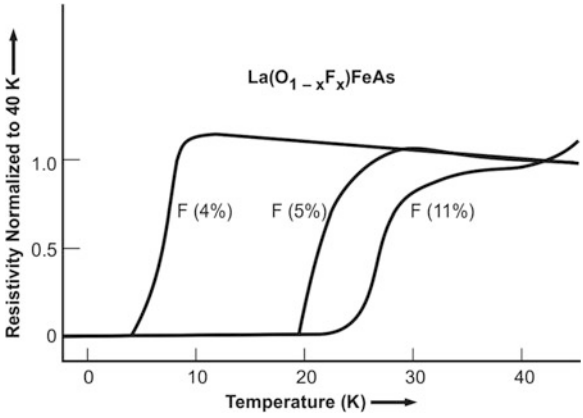

Fig. 4.24 Electrical resistivity plotted against temperature for La($O_{1-x}F_x$) FeAs for 0, 4, 5 and 11 %) of F-doping [56] (With permission from American Chemical Society)

the un-doped samples are $a = 0.403552(8)$ nm and $c = 0.87263(3)$ nm. The lattice constants decrease with F-doping. Thus for example, the lattice parameters for 5 % F-doping are: $a = 0.40320(1)$ nm and $c = 0.87263(3)$ nm.

The electrical resistivity of La($O_{1-x}F_x$)FeAs are plotted against temperature up to 40 K in Fig. 4.24. The un-doped sample does not show superconductivity down to the lowest temperature. Samples with F 4 % and above doping show superconductivity

between 5 and 22 K. Highest value of T_c (=26 K) is obtained for 11 at.% F-doped sample. Higher doping leads to a drop in T_c. Similar results on superconducting transition have been obtained from susceptibility measurements. The value of χ_{mol} for the 5 % F-doped sample starts decreasing at 25 K and is negative, confirming the onset of superconductivity.

Another interesting finding of these studies is that superconductivity was not observed when doping was done with Ca^{2+} instead of with F. This gives a strong signal that superconductivity is induced by electron (F^-)-doping and not by hole (Ca^{2+})-doping. The material LaOFeAs was prepared following the solid state method. Powders of dehydrated La_2O_3, lanthanum arsenide and iron arsenide were thoroughly mixed and sealed in a silica tube filled with Ar-gas. The tube was heated to 1,250 °C for 40 h. Right quantities of CaO and 1:1 mixture of LaF_3 and La were added to the starting material for doping with Ca^{2+} and F^- respectively. This was followed again by the same heating schedule.

4.7.2 High T_c (>50 K) in Sm and Nd Based Oxypnictides

Significantly, high values of T_c have been reported for these oxypnictides by replacing La by different rare earths. For Ce-compound the T_c rises to above 40 and 50 K for Nd, Pr, Sm and Gd. Jaroszynski et al. [57] reported T_c higher than 50 K for their Sm and Nd based materials. They carried out high field studies on three REFeAsO(1111) materials with RE as La, Sm and Nd. Superconductivity was induced either by doping F at O-sites or creating O-vacancies by synthesizing O-deficient materials. Three compounds studied, viz; $LaFeAsO_{0.89}F_{0.11}$, $SmFeAsO_{0.85}F_{0.15}$ and $NdFeAsO_{0.94}F_{0.06}$ yield T_c = 28, 53.5 and 50.5 K respectively. These values have been tabulated in Table 4.5. It is to be mentioned that these materials were synthesized at high pressure and high temperature following the solid state reaction route. Pre-sintered powders of LaAs. SmAs and NdAs were mixed together with powders of Fe, Fe_2O_3 and FeF_2 in right stoichiometric proportions ground and pressed into pellet form. The pellets were sealed in BN (boron nitride) tubes and heated at 1,250 °C under 6 GPa pressure for 2 h. Interestingly, the highest values of T_c obtained for optimal doping show that the optimal level is different for different doping materials, viz; 11, 15 and 6 % for La, Sm and Nd respectively. A detailed review article on oxypnictides has recently appeared in the literature [58].

Table 4.5 Superconducting parameters of REFeAsO(1111) oxypnictides with RE as La, Sm and Nd [57]

Parameter	Unit	$LaFeAsO_{0.89}F_{0.11}$	$SmFeAsO_{0.85}F_{0.15}$	$NdFeAsO_{0.94}F_{0.06}$
Transition temperature, T_c	K	28	53.5	50.5
Optimum doping of F	%	11	15	6
Upper critical field, B_{c2}	T	36	150	204

Table 4.6 Superconducting parameters of REFeAsO (1111) oxypnictides with RE as La, Sm, Nd, Pr and Ce [61]

Oxypnictide	T_c (K)	B_{c2} (0 K)
$LaFeAsO_{0.89}F_{0.11}$		36
$SmFeAsO_{0.85}F_{0.15}$		150
$NdFeAsO_{0.94}F_{0.06}$		204
$PrFeAsO_{0.94}F_{0.06}$		72
$CeFeAsO_{0.8}F_{0.2}$	42.5	43
$CeFeAsO_{0.9}F_{0.1}$	38.4	94
$NdFeAsO_{0.82}F_{0.18}$ [58]	51	230

The upper critical field B_{c2} of La $FeAsO_{1-x}F_x$ (1111) compounds turns out to be high. The B_{c2} values as evaluated from resistive (ρ-B plots) using Werthamer-Helfend-Hohenberg (WHH) formula,

$$B_{c2} = -0.693 T_c [dB_{c2}/T]_{T_c} \tag{4.5}$$

and extrapolated to 0 K for La, Sm, Nd, Pr, and Ce(1111) compounds are [61] 36, 150, 204, 72 and 107 T respectively (Table 4.6). B_{c2} has been found to decrease with increasing F^- doping even though T_c shows an opposite trend. For $CeFeAsO_{0.8}F_{0.2}$ the B_{c2} is 43 T and T_c is 42.5 K and for $CeFeAsO_{0.9}F_{0.1}$ the B_{c2} value is 94 T and T_c is 38.4 K. Similar variation of B_{c2} is reported for $LaFeAsO_{1-x}F_x$. For $LaFeAsO_{0.95}F_{0.05}$ the B_{c2} is 63–65 T and for $LaFeAsO_{0.89}F_{0.11}$ it is 73 T. Sm(1111) compound also show similar behaviour. Like the T_c of this compound B_{c2} of the (1111) compounds also increases if the compound is prepared by high pressure route. B_{c2} up to 230 T and T_c of 51 K have been reported [58] in $NdFeAsO_{0.82}F_{0.18}$. The field anisotropy B_{c2ab}/B_{c2c} is about five, much smaller than in YBCO compound. The values of irreversible field, B_{irr} are also correspondingly high as compared to MgB_2. Above tables indicate beyond doubt that these materials can have high T_c and B_{c2} once the parameters are optimized.

In spite of high B_{c2} and high T_c these compounds suffer from the problem of granularity similar to cuprates. Thus the inter-grain critical current J_{cgb} is far smaller than the intra-grain critical current J_{cg}. Through magneto-optical measurements (low temperature laser scanning electron microscopy) on Sm(1111) compounds Kametani et al. [59] have shown that the transport current though is high within the grains but is low at the grain boundary in very low field. The grain boundaries are identified as Fe–As normal wetting phase surrounding Sm(1111) grains. These grain boundaries produce a dense array of Josephson-coupled superconducting-normal-superconducting (SNS) junctions. Transport J_c of $SmFeAsO_{0.85}$, prepared by high pressure technique drops sharply with small magnetic field. The authors had earlier established that the irreversible field B_{irr} at 39 K in this material is 25 T. J_c, nearly independent of field between 1 and 5 T does support this observation. The self field transport J_c obtained is 463 A cm^{-2} at 39 K and whole-sample global J_c of 600 A cm^{-2} are consistent with each other. Authors also observe fine micro-cracks along the grain boundaries which too must lower the transport J_c. It is fair to

conclude that to exploit these materials for practical applications more efforts are required to get rid of the unwanted Fe–As normal metal wetting phase and the micro-cracks.

4.7.3 Superconductivity in K-Doped $BaFe_2As_2$(122) Compounds

A new member of the Fe–As superconductor family was discovered in 2008 shortly after the discovery of superconductivity in LaFeAsO system at 26 K through F-doping and raising the T_c to all time high 55 K in $SmFeAsO_{1-x}$ system. This was achieved by F^-doping or creating oxygen deficiency (electron-doping) in the Fe_2As_2 conducting layer which suppresses the structure phase transition (at 135–140 K) and induces superconductivity. Hole doping too has been reported to induce superconductivity in the $(La_{1-x}Sr_x)FeAsO$ system but the T_c was limited to 25 K.

Rotter et al. [60] discovered superconductivity first time in an oxygen free pnictide. A T_c of 38 K has been reported in a compound, $(Ba_{0.6}K_{0.4})Fe_2As_2$ prepared by partially replacing Ba with K. The parent compound $BaFe_2As_2$ has a tetragonal $ThCr_2Si_2$ type crystal structure with I4/mmm space group and consisting of $(FeAs)^-$ layers separated by Ba^{2+} ions as shown in Fig. 4.25. $BaFe_2As_2$ is a poor metal with Pauli paramagnetism. It shows a spin density wave (SDW) anomaly at 140 K similar to the anomaly in LaFeAsO compound at 150 K. The anomaly is accompanied with a structural and magnetic phase transition and anomalous specific heat, resistivity and susceptibility. Hole doping in $(FeAs)^-$ layers by partial substitution of K^+ on the Ba^{2+} sites suppresses this SDW anomaly and induces superconductivity. This SDW anomaly seems to be a pre-requisite for superconductivity. The structural phase transition can be suppressed by electron-doping or hole-doping in the Fe–As layer which leads to the appearance of superconductivity. Through this Substitution, the authors [60] have found superconductivity in $(Ba_{0.6}K_{0.4})Fe_2As_2$ at 38 K. The resistive superconducting transition is shown in Fig. 4.26. Thus a new category of oxygen-free Fe–As compounds was added to the list of Fe–As based superconductors.

4.7.4 Superconductivity in Iron-Chalcogenides and Mysterious Behaviour at High Pressures

After the discovery of superconductivity in Fe-oxypnictides of the type LaFeAsO these compounds became the most studied materials with an object of getting higher T_c. Report of T_c as high as 55 K in oxygen-deficient $SmFeAsO_{0.85}$ [57] inspired researchers to continue to look for Fe-based superconductors with still

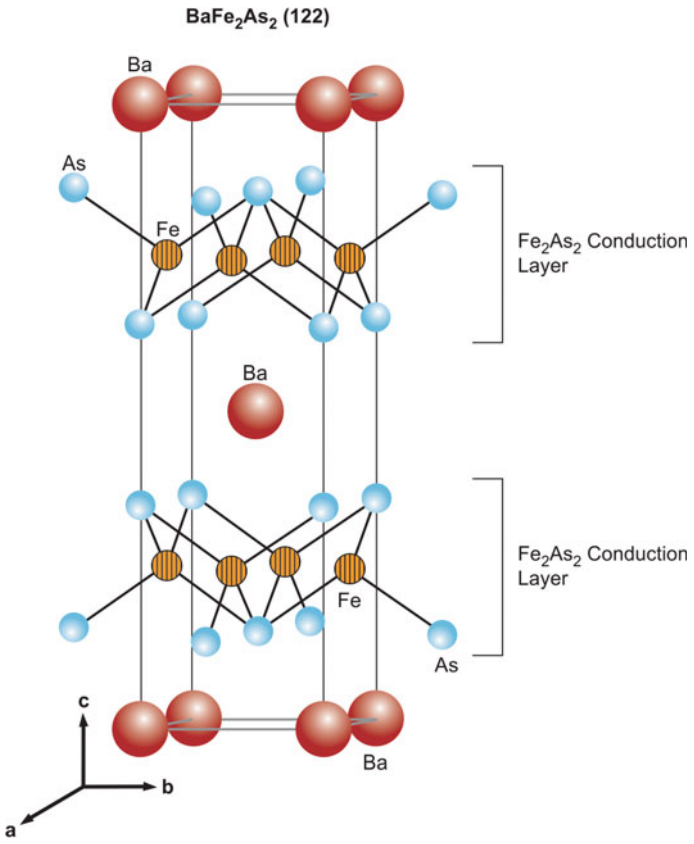

Fig. 4.25 Crystal structure of $BaFe_2As_2$(122) compound (of the type $ThCr_2Si_2$) with space group I4/mmm [60]. (With permission from APS) http://journals.aps.org/prb/abstract/10.1103/PhysRevB.82.180520

higher T_c. Superconductivity was indeed reported in a new material, Fe–Se or referred to as [11] iron-chalcogenide at 8 K by Hsu et al. [61]. This compound has a simple structure of Fe–Se layers without intercalating cations, something quite different from the oxypnictides. Static magnetic ordering too does not occur up to a pressure of 38 GPa. Tellurium doping ($FeSe_{0.42}Tl_{0.58}$) raises the T_c to 15 K and the high pressure up to 37 K. Guo et al. [62] reported superconductivity in a compound of the composition $K_{0.8}Fe_2Se_2$ at 30 K at ambient pressure. The compound was synthesized through intercalation of Fe–Se by K. Figure 4.27 shows the crystal structure of this compound. Single crystal grown by flux method shows a tetragonal structure with a = 3.9136(1) Å and c = 14.0367(7) Å and space group I4/mmm. Obviously, the intercalation increases the c-axis parameter significantly. The carrier density as evaluated from Hall effect measurement turns out to be $1.76 \times 10^{21}/cm^3$. The Hall coefficient R_H is negative and constant above 105 K. The electrical conduction is thus electron dominated. The compound has a semiconductor

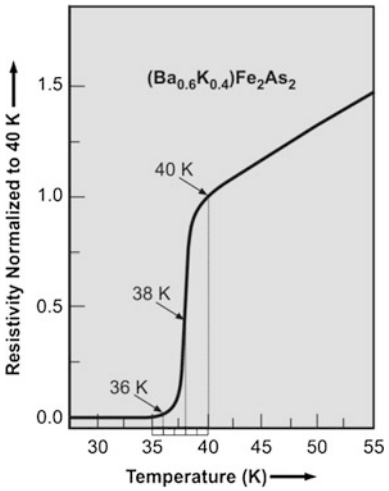

Fig. 4.26 Resistive superconducting transition in $(Ba_{0.6}K_{0.4})Fe_2As_2$ [60]. (With permission from APS) http://journals.aps.org/prb/abstract/10.1103/PhysRevB.82.180520

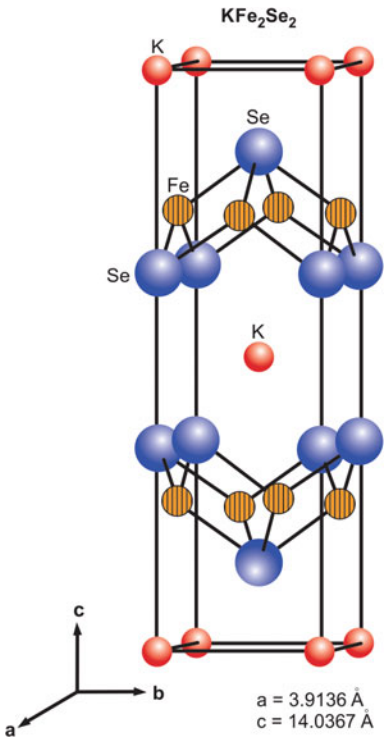

Fig. 4.27 The crystal structure of KFe_2Se_2 of the type ($ThCr_2Si_2$) a = 3.9136 (1) Å and c = 14.0367 Å [62]. (With permission from APS) http://journals.aps.org/prb/abstract/10.1103/PhysRevB.82.180520

behaviour in electrical resistivity between room temperature and 105 K below which it turns metallic and finally superconducting (at 30 K). The resistive transition of the $K_{0.8}Fe_2Se_2$ compound is shown in Fig. 4.28. The lower critical

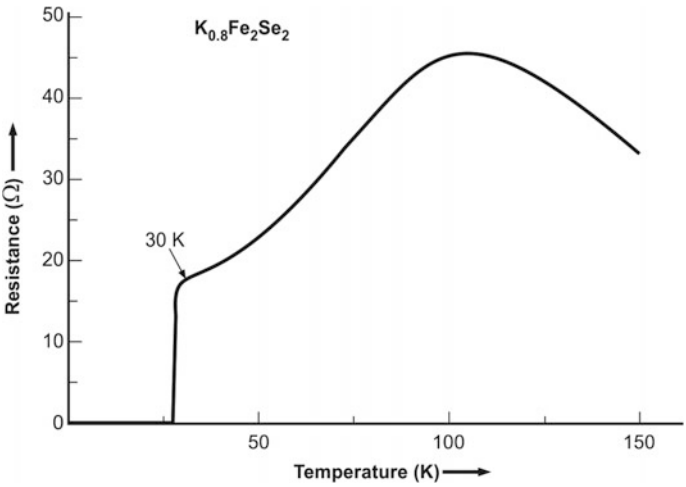

Fig. 4.28 Resistance/temperature behaviour of $K_{0.8}Fe_2Se_2$, below 150 K. Superconducting transition occurs at 30 K [62]. (With permission from APS) http://journals.aps.org/prb/abstract/10.1103/PhysRevB.82.180520

magnetic field B_{c1} and upper critical magnetic field B_{c2} have been calculated to be 0.2 and 9 T respectively.

A mysterious behaviour of repeat appearing and disappearing of superconductivity in iron-chalcogenide has been reported very recently by Sun et al. [63]. They probed the basic electronics and structural properties of iron-chalcogenides by the application of pressure. Pressure application is perhaps the cleanest way to probe such properties. They carried out their studies on the single crystals of $(Tl_{0.6}Rb_{0.4})Fe_{1.67}Se_2$, $K_{0.8}Fe_{1.7}Se_2$ and $K_{0.8}Fe_{1.78}Se_2$ grown by the Bridgman technique and conducted resistivity and magnetic susceptibility measurements at low temperature and under varying applied pressure. The results shown in Fig. 4.29 were stunning. Superconductivity for example in the compound $Tl_{0.6}Rb_{0.4}Fe_{1.67}Se_2$, $K_{0.8}Fe_{1.7}Se_2$ sets-in at an optimum pressure of 1.6 GPa with a T_c of 33 K, T_c decreases with increasing pressure and superconductivity vanishes at a pressure of 9 GPa. What was astounding, was that while the pressure was raised further beyond 9 GPa superconductivity again surfaced at 48 K, an high T_c indeed, at a pressure of 12.4 GPa. There seem to be two distinct superconducting phases in this material. One can call them the superconducting phase I and phase II respectively. These superconductors possess rather high magnetic moment something like 3.3 μ_B per Fe atom and have Fe-vacancy ordering in the Fe square lattice. Existence of superconductivity in materials with such high magnetic moment is a riddle to be sorted out. Quite similar behaviour has been observed in other two systems, namely, $K_{0.8}Fe_{1.7}Se_2$ and $K_{0.8}Fe_{1.78}Se_2$. This type of re-emergence of superconductivity has been found earlier in strongly correlated electron systems like heavy-Fermions [64] and some organic systems [65]. It appears that by manipulating the thermodynamical parameters like pressure, T_c can be raised to high values hitherto not attainable.

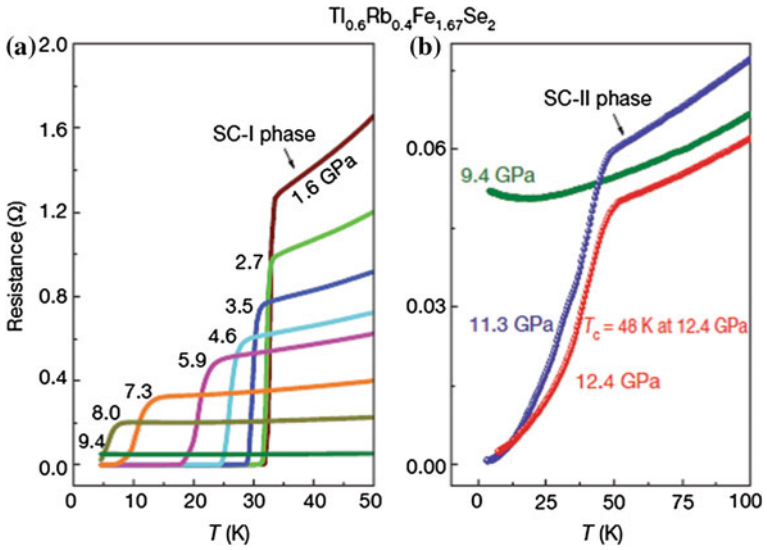

Fig. 4.29 The resistivity-temperature plots of $Tl_{0.6}Rb_{0.4}Fe_{1.67}Se_2$ at varying pressures. **a** Superconductivity occurs at 33 K at a pressure of 1.6 GPa and disappears at a pressure of 9 GPa. **b** A second phase of superconductivity sets-in at a pressure of 12.4 GPa. The compound looses superconductivity at a still higher pressure of 13.2 GPa [63]. (With permission from Nature Publishing Group)

References

1. J.R. Gavaler, Appl. Phys. Lett. **23**, 480 (1974)
2. L.R. Tastardi, J.H. Wernick, W.A. Royer, Solid State Commun. **15**, 1 (1974)
3. J.G. Bednorz, K.A. Muller, Z. Phys. B: Condens. Matter **64**, 189 (1986)
4. D.C. Johnston, H. Prakash, W.H. Zachariasen, R. Viswanathan, Mater. Res. Bull. **8**, 777 (1973)
5. A.W. Sleight, J.L. Gillson, F.E. Bierstedt, Solid State Commun. **17**, 27 (1975)
6. C.W. Chu, P.H. Hor, R.L. Meng et al., Phys. Rev. Lett. **58**, 405 (1987)
7. R.J. Cava, R.B. van Dover, B. Batlogg, E.A. Rietman, Phys. Rev. Lett. **58**, 408 (1987)
8. R.P. Aloysius, Ph.D. thesis, Cochin University of Science and Technology, Cochin (2002)
9. M.K. Wu, J.R. Ashburn, C.J. Torng et al., Phys. Rev. Lett. **58**, 908 (1987)
10. R.G. Sharma, Y.S. Reddy, S.R. Jha, S.S. Dubey, Pramana-J. Phys. **30**, L-81 (1988)
11. S.R. Jha, Y.S. Reddy, D.K. Suri, K.D. Kundra, R.G. Sharma, D. Kumar, Pramana-J. Phys. **32**, 277 (1989)
12. A. Pandey, R. Rajput, B. Sarkar, Y.S. Reddy, R.G. Sharma, Physica **C256**, 335 (1996)
13. A. Pandey, Y.S. Reddy, R.G. Sharma, J. Mater. Sci. **32**, 3701 (1997)
14. R.G. Sharma, S. Lahiry, A. Pandey, D. Bhattacharya, Bull. Mater. Sci. **22**, 265 (1999)
15. R.G. Sharma, Y.S. Reddy, S.R. Jha, Rev. Solid State Sci. **2**, 409 (1988)
16. P. Chaudhuri, R.H. Koch, R.B. Laibowitz et al., Phys. Rev. Lett. **58**, 2684 (1987)
17. T.R. Dinger, T.K. Worthington, W.J. Gallagher, R.L. Sandstorm, Phys. Rev. Lett. **58**, 2687 (1987)
18. H. Maeda, Y. Tanaka, M. Fukutomi, T. Asano, Jpn. J. Appl. Phys. **27**, L665 (1987)
19. M. Takano, J. Takada, K. Oda et al., Jpn. J. Appl. Phys. **27**, L1652 (1988)

20. B. Sarkar, Y.S. Reddy, R.G. Sharma, Mater. Res. Bull. **28**, 629 (1993)
21. S.R. Shukla, D.K. Pandya, N. Kumar, S.K. Sharma, R.G. Sharma, Physica **C219**, 483 (1994)
22. S.R. Shukla, Y.S. Reddy, N. Kumar, S.K. Sharma, R.G. Sharma, Pramana-J. Phys. **41**, 285 (1993)
23. H. Maeda, K. Innoue, T. Kiyoshi, T. Asano et al., Phys. B **216**, 141 (1996)
24. M. Tachiki, S. Takahashi, Solid State Commun. **70**, 291 (1989)
25. K. Kadowaki, in *Electronic Properties and Mechanism of High T_c Superconductors,* ed. by T. Oguchi, K. Kadowaki, T. Sasaki (North-Holland, Amsterdam, 1992), p. 209
26. M. Kikuchi, N. Ayai, T. Ishida et al., SEI Tech. Rev. **66**, 73 (2008)
27. Z.Z. Sheng, A.M. Hermann, Nature **332**, 55 (1988)
28. Z.Z. Sheng, A.M. Hermann, Nature **332**, 138 (1988)
29. S.S.P. Parkin, V.Y. Lee, E.M. Engler et al., Phys. Rev. Lett. **60**, 2539 (1988)
30. S.N. Putillin, E.V. Antipov, O. Chmaissem, M. Marezio, Nature **362**, 226 (1993)
31. A. Schilling, M. Cantoni, J.D. Guo, H.R. Ott, Nature **363**, 56 (1993)
32. C.W. Chu, L. Gao, F. Chen et al., Nature **365**, 323 (1993)
33. L. Gao, Y.Y. Xue, F. Chen et al., Phys. Rev. **B50**, 4260 (1994)
34. E.V. Antipov, A.M. Abakumav, S.N. Putillin, Supercond. Sci. Technol. **15**, R-31 (2002)
35. J. Nagamatsu, N. Nakagawa, T. Muranaka et al., Nature **410**, 63 (2001)
36. R. Nagarajan, C. Mazumdar, J. Hossain et al., Phys. Rev. Lett. **72**, 274 (1994)
37. R. Cava, H. Takagi, H.W. Zandbergen et al., Nature **367**, 252 (1994)
38. H.J. Choi, D. Roundy, H. Sun, M.L. Cohen, Nature **418**, 758 (2002)
39. R.S. Gonelli, A. Calzolari, D. Deghero et al., Phys. Rev. Lett. **87**, 097001 (2001)
40. C. Buzea, T. Yamashita, Supercond. Sci. Technol. **14**, R 115 (2001)
41. K. Vinod, N. Verghese, U. Syamaprasad, Supercond. Sci. Technol. **20**, R31 (2007)
42. K. Vinod, R.G. Abhilash Kumar, U. Syamaprasad, Supercond. Sci. Technol. **20**, R1 (2007)
43. J. Kapinski, S.M. Kazakov, J. Jun et al., Phys. C (Supercond.) **385**, 42 (2003)
44. K. Komori, K. Kawagishi, Y. Takano et al., Appl. Phys. Lett. **82**, 1047 (2002)
45. V. Ferrando, P. Orgiani, A.V. Pogrebnyakov et al., Appl. Phys. Lett. **87**, 252509 (2005)
46. G. Glasso, A. Malagoli, C. Ferdeghini et al., Cond-Mat/0103563
47. H. Kumakura, A. Matsumoto, H. Fuji, K. Togano, Appl. Phys. Lett. **79**, 2435 (2001)
48. H. Fang, P.T. Putman, S. Padmanabhan et al., Supercond. Sci. Technol. **17**, 717 (2004)
49. M.D. Sumption, M. Bhatia, X. Wu et al., Supercond. Sci. Technol. **18**, 730 (2005)
50. Y. Elstev, K. Nakao, S. Lee et al., Phys. Rev. B **66**, 180504 (2002)
51. S.L. Bud'ko, G. Labertot, C. Petrovic, et al., Phys. Rev. Lett. **86**, 1877 (2001)
52. B. Lorenz, R.L. Meng, C.W. Chu, Phys. Rev. B **64**, 012507 (2001)
53. S. Patnaik, L.D. Cooley, A Gurevich, et al., Supercond. Sci. Technol. **14**, 315 (2001)
54. V. Braccini, A. Gurevich, J.E. Giencke et al., Phys. Rev. B **71**, 012504 (2005)
55. Y. Kamihara, H. Hiramatsu, M. Hirano et al., J. Am. Chem. Soc. **128**, 10012 (2008)
56. Y. Kamihara, T. Watanabe, M. Hirano, H. Hosono, J. Am. Chem. Soc. **130**, 3296 (2008)
57. J. Jaroszynski, C. Scott, F. Riggs et al., Phys. Rev. B **78**, 064511 (2008)
58. P.M. Aswathy, J.B. Anuja, P.M. Sarun, U. Syamaprasad, Supercond. Sci. Technol. **23**, 073001 (2010)
59. F. Kametani, P. Li, D. Abrrimov et al., Appl. Phys. Lett. **95**, 142502 (2009)
60. M. Rotter, M. Tegel, D. Johrendt, Phys. Rev. Lett. **101**, 107006 (2008)
61. F.C. Hsu, J.U. Luo, K.W. Yeh et al., Proc. Natl. Acad. Sci. U.S.A. **105**, 14262 (2008)
62. J. Guo, S. Jin, G. Wang et al., Phys. Rev. B **82**, 180520(R) (2010)
63. L. Sun, X.J. Chen, J. Guo et al., Nature **483**, 67 (2012)
64. H.Q. Yuan, F.M. Groche, M. Deppe et al., Science **302**, 2104 (2003)
65. T. Okuhata, T. Nagai, H. Taniguchi et al., J. Phys. Soc. Jpn. **76**(Suppl. A), 188 (2007)